

AD-A124 708

CHARACTERIZATION OF A PULSED HF OPTICAL RESONANCE

1/2

TRANSFER LASER(U) AIR FORCE INST OF TECH

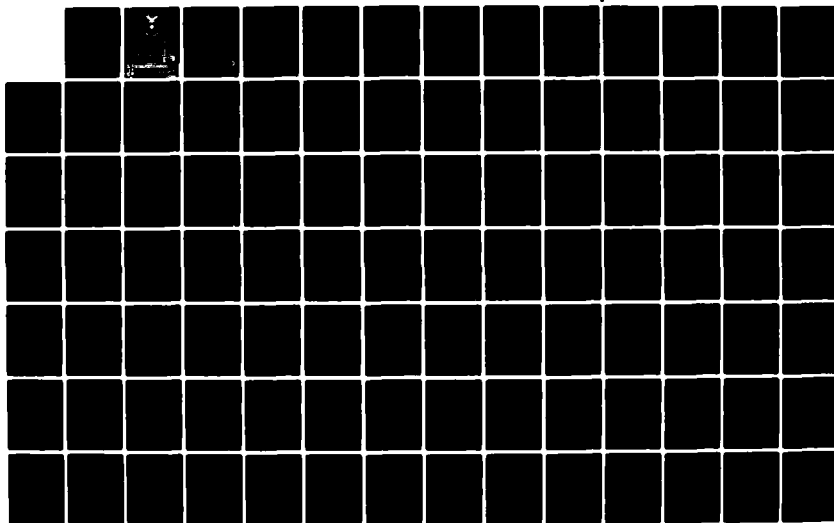
WRIGHT-PATTERSON AFB OH SCHOOL OF ENGINEERING D A RUDD

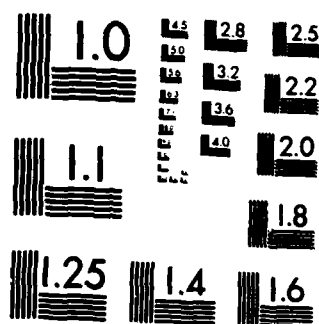
UNCLASSIFIED

OCT 82 AFIT/GEP/PH/82D-20

F/G 20/5

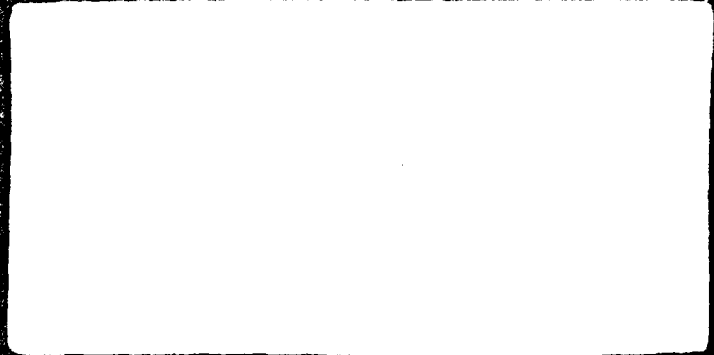
NL





MICROCOPY RESOLUTION TEST CHART
NATIONAL BUREAU OF STANDARDS-1963-A

ADA 124708



CHARACTERIZATION OF A PULSED HF
OPTICAL RESONANCE TRANSFER LASER

THESIS

AFIT/GEP/PH/82D-20

Douglas A. Rudd
1st Lt USAF

OTIC
ECTE
FEB 22 1983

A

This document has been approved
for public release and sale; its
distribution is unlimited.

CHARACTERIZATION OF A PULSED HF
OPTICAL RESONANCE TRANSFER LASER

THESIS

Presented to the Faculty of the School of Engineering
of the Air Force Institute of Technology
Air University
in Partial Fulfillment of the
Requirements for the Degree of
Master of Science

by

Douglas A. Rudd, B.S.

1st Lt

USAF

Graduate Engineering Physics

October 1982



Preface

The purpose of this study was to characterize the performance of a Pulsed HF Optical Resonance Transfer Laser, measuring gain and absorption as a function of temperature and time. The resultant data is then analyzed and compared to the theoretical kinetic models. A comparison is made to previous work done with the Pulsed HF Optical Resonance Transfer Laser.

I would like to acknowledge the support of the Avionics Laboratory, AFWL, WPAFB, OH in conducting this study, particularly Dr. W. Schuebel for sponsoring the project and J. Brandelik for his guidance and advice. The support of my AFIT thesis advisor, Dr. E. A. Dorko, and thesis committee members, Dr. W. B. Roh and Lieutenant Colonel J. H. Erkkila was greatly appreciated. Discussions and information provided by Dr. D. Drummond, AFWL was also greatly appreciated. The technical support provided by C. Shortt, AFIT Shop supervisor, S. Derby, Avionics Lab, J. R. Gabriel, AFIT, is gratefully acknowledged.

Contents

	Page
Preface	ii
List of Figures	v
List of Tables	vii
Abstract	viii
I. Introduction	1
II. Background Theory	3
HF Laser Spectroscopy	3
Kinetics Model for HF	7
III. Experiment	23
Gas System	23
Optical Train	26
Electronics	29
ORTL Experiment	32
HF Pump Laser	33
Laser Safety	36
Alignment Procedures for the Optical Train	38
IV. Results and Conclusions	40
Monochromater Calibration and Line Identification	40
ORTL Experiment	44
Kinetics Modeling	58
Conclusions and Recommendations	72
Bibliography	74
Appendix A: HF Lumonics Model TE-112 Laser Operating Instructions	78
Appendix B: Computer Program Listings	79
Appendix C: Electronic Equipment Listings/ Settings for Boxcar Averager	82
Appendix D: Fresnel's Equations	83

Contents

	Page
Appendix E: Temperature of the Gas in the ORTL Cell	85
Appendix F: Retractive Index Calculations	86
Appendix G: Photon Number Calculations	87

List of Figures

<u>Figure</u>	<u>Page</u>
1 Energy Level Diagram for HF	6
2 Potential Energy Diagram for $A+B \rightarrow AB$	7
3 Potential Energy Diagram for $A+BC \rightarrow AB+C$	8
4 Potential Energy Diagram for $F+H_2 \rightarrow H+HF$	11
5 V-V, Dissociation Species	21
6 HF Spectra	22
7 Gas System	24
8 Optical Train	27
9 Pump/Probe Train Detail	28
10 Electronics	30
11 HF Probe Pulse Shapes (AFWL)	42
12 HF Probe Line Averages	43
13 Helium and HF/Helium Time Average Over Pulse $P_2(8)$ (A) . . .	46
14 Helium and HF/Helium Time Average Over Pulse $P_2(8)$ (B) . . .	47
15 Discrete Time Average: Helium $P_2(8)$	49
16 Discrete Time Average: HF/Helium (Pump on) $P_2(8)$	50
17 Discrete Time Average: HF/Helium (Pump off) $P_2(8)$	51
18 Helium Time Average Over Pulse $P_2(8)$ (Pump on) Ratio	53
19 HF/Helium Time Average Over Pulse $P_2(8)$ (Pump on) Ratio . . .	54
20 HF/Helium Time Average Over Pulse $P_2(8)$ (Pump off) Ratio . .	55
21 Decreased-Increased Absorption vs Time $P_2(8)$	56

<u>Figure</u>		<u>Page</u>
22	Gain-Loss vs Time $P_2(8)$ (AFWL)	57
23	Helium Time Average Over Pulse $P_2(7)$ Ratio	59
24	HF/Helium Time Average Over Pulse $P_2(7)$ (Pump on) Ratio . .	60
25	HF/Helium Time Average Over Pulse $P_2(7)$ (Pump off) Ratio . .	61
26	Decreased-Increased Absorption vs Time $P_2(7)$	62
27	Gain-Loss vs Time $P_2(7)$ (AFWL)	63
28	Pump Beam Leakage into Probe Path $P_2(8)$	64
29	Decreased-Increased Absorption vs Time $P_2(8)$ from Table IV Data	65
30	Rate Equation Plot: N_2	67
31	Rate Equation Plot: N_1	68

List of Tables

<u>Table</u>		<u>Page</u>
I	HF Laser Lines	33
II	Observed HF Lines	41
III	HF Lines Not Observed	41
IV	Discrete Time Average Over Pulse $P_2(8)$	48
V	Numerical Solution of Rate Equations	69
VI	Boxcar Averager Settings	82

Abstract

The HF ($v=2$) vibrational level was pumped optically on the $P_2(8)$ transition and $P_2(7)$ transition. The 0.5 percent HF in helium gas at 50 torr was pumped by an HF laser with 0.081 joules per pulse and 96 pulses per second. The technique involves observation of absorption by HF ($v=2$). Decreased absorption was observed on the $P_2(8)$ transition implying the possibility of gain by V-V exchange. The data shows conformance with the results of a previous investigation on the $P_2(8)$ line. Interrogation of the $P_2(7)$ transition failed to yield conclusive results due to a poor signal to noise ratio.

A theoretical model of the kinetics of the HF V-V and V-T exchanges was established. Pulse shapes predicted by this theory and those observed experimentally for the $P_2(8)$ line agree well.

Excessive noise levels precluded investigation of other transitions.

Introduction

Background

Laser sources are needed that cover a wide range of the electromagnetic spectrum. Future Air Force missions will require such sources in the three to five micrometer wavelength region. The Optical Resonance Transfer Laser (ORTL) is a method by which the inherent spectral output of HF and DF can be translated into that region. Optical Resonance Transfer pumping occurs by optical pumping of a molecule which does not lase. The vibrational energy of the pumped molecule is transferred by collision to a vibrational mode of another molecule (the lasing species). The multimode operation of the chemical laser acting as a pump laser are no longer detrimental as the pump laser acts as a source of optical power only. The output beam control function is now transferred to the ORTL [17:1], [1:68-69]. Most studies to date have centered on the continuous wave (CW) ORTL [2:1-3], [3:1-3], [4:912-913], [5:24]. The pulsed ORTL has been investigated by Dr. Drummond [6] at the Air Force Weapons Laboratory (AFWL), working at room temperatures. The results of the AFWL work appear to contradict established theory.

Problem Definition

This investigation will measure gain and absorption of a Hydrogen Fluoride (HF) ORTL cell as a function of time and to reproduce the work of reference [6]. The experimental results will be analysed and

compared with the results of previous work [6]. The work done by Dr. Drummond shows little or no gain on the lines investigated [6]. A larger gain than found would be expected on theoretical grounds. The primary effort of this thesis is to explain this discrepancy between theory and experiment.

Presentation

Background theory on the operation of the pulsed HF ORTL will be presented in Chapter II and a kinetic model of the ORTL will be established. Chapter III will describe the ORTL experimental setup and power requirements of the HF pump laser. Chapter IV will present the results of the investigation of loss/gain in the ORTL. Conclusions concerning the previous work at AFWL [6] and the present study will be drawn. Recommendations for future studies and future work are then made.

Background Theory

The main topics covered in this chapter are: (1) spectroscopy of the HF laser and (2) a kinetic model of HF vibrational, rotational and translational states including a kinetic model of the HF pump laser. The purpose is to develop the background needed to understand the Optical Resonance Transfer Laser (ORTL) spectroscopy and kinetics and the interaction of the pump laser with the HF/He gas in the ORTL cell.

HF Laser Spectroscopy

Chemical lasing action was first demonstrated in 1965 by Kasper and Pimentel [7:352-354] and an HF chemical laser was first reported by Kompa and Pimentel [8:857-858].

The HF molecule can be modeled for lower vibrational energies by a simple nonrotating ball and spring system. The potential function for this model is used in the Schrödinger equation assuming the harmonic oscillator model for vibrational motion in a diatomic molecule. The energies are found to exist in discrete quanta, where

$$E_v = (v + \frac{1}{2})\omega h c, v=0,1,2,\dots$$

and ω is the vibrational constant. This model is assumed in later development of the pump laser pulse characteristics [9:15-16].

A better approximation to the potential well is the Morse potential [10]:

$$V(x) = D e q \{1 - \exp(ax)\}^2$$

where $a = \text{constant}$

$D_{eq} = \text{Dissociation energy}$

$$x = r_{eq} - r$$

using this expression in the Schrödinger equation and solving for the energy eigen values

$$E_v = (v + \frac{1}{2})\bar{\omega}_e - (\bar{v} + \frac{1}{2})^2 \bar{\omega}_e x_e$$

where $\bar{\omega}_e = \frac{\omega}{2\pi c} = \frac{v}{c}$

and $x_e = \frac{h\nu}{4D_{eq}}$

extending this model to HF with its large anharmonicity, further accuracy is obtained using the equation [10]:

$$E_v = (v + \frac{1}{2})\bar{\omega}_e [1 - x_e(v + \frac{1}{2}) + y_e(v + \frac{1}{2})^2 - z_e(v + \frac{1}{2})^3]$$

where

$$\begin{aligned}\bar{\omega}_e &= 4138.52 \text{ cm}^{-1} \\ x_e \bar{\omega}_e &= 90.06 \text{ cm}^{-1} \\ y_e \bar{\omega}_e &= 0.980 \text{ cm}^{-1} \\ z_e \bar{\omega}_e &= 0.025 \text{ cm}^{-1}\end{aligned}$$

This model is used in a computer model used to verify rate constants in the kinetics development.

A rigid rotator can be assumed for a rotational model for the HF molecule [10]. For this model

$$H = \frac{1}{2} I \omega^2 = \frac{1}{2} \frac{J^2}{I}$$

$$\text{or } \hat{H} = \frac{1}{2I} \hat{J}^2$$

$$\text{then } \hat{H}\psi = E\psi$$

$$\text{and } E_J = \frac{J(J+1) h^2}{8\pi^2 I}$$

$$\text{or } E_J = BJ(J+1)$$

$$\text{where } B = h^2/8\pi^2 Ic$$

a nonrigid rotator, however, provides a more accurate model with energy eigen values

$$E_J = J(J+1) h^2/2I - J^2(J+1)^2 h^4/2kI^2 r_o^2$$

$$\text{or } E_J = \frac{E_J}{hc} = BJ(J+1) - D J^2(J+1)^2$$

where k = retarding force constant

r_o = rest position of molecule

$$D = h^3/(32\pi^4 I^2 r_o^2 k) \quad [10].$$

Diatomic molecular lasers such as HF and DF lasers utilize vibrational-rotational transitions between levels. Figure 1 shows P branch transitions which are of interest in this investigation. $P_v(J)$ denotes $(v, J-1) \leftrightarrow (v-1, J)$ vibrational rotational transition. The vibrational levels are indicated by horizontal lines. The blow up shows the rotational lines for the low lying vibrational states and the electronic ground state.

The line widths of HF $P_v(J)$ lines are of interest as they will determine the amount of power that can be absorbed by the HF molecules in the ORTL cell and the character of the absorption.

Three types of spectral broadening are of concern: natural, collisional, and doppler broadening. Natural or resonance

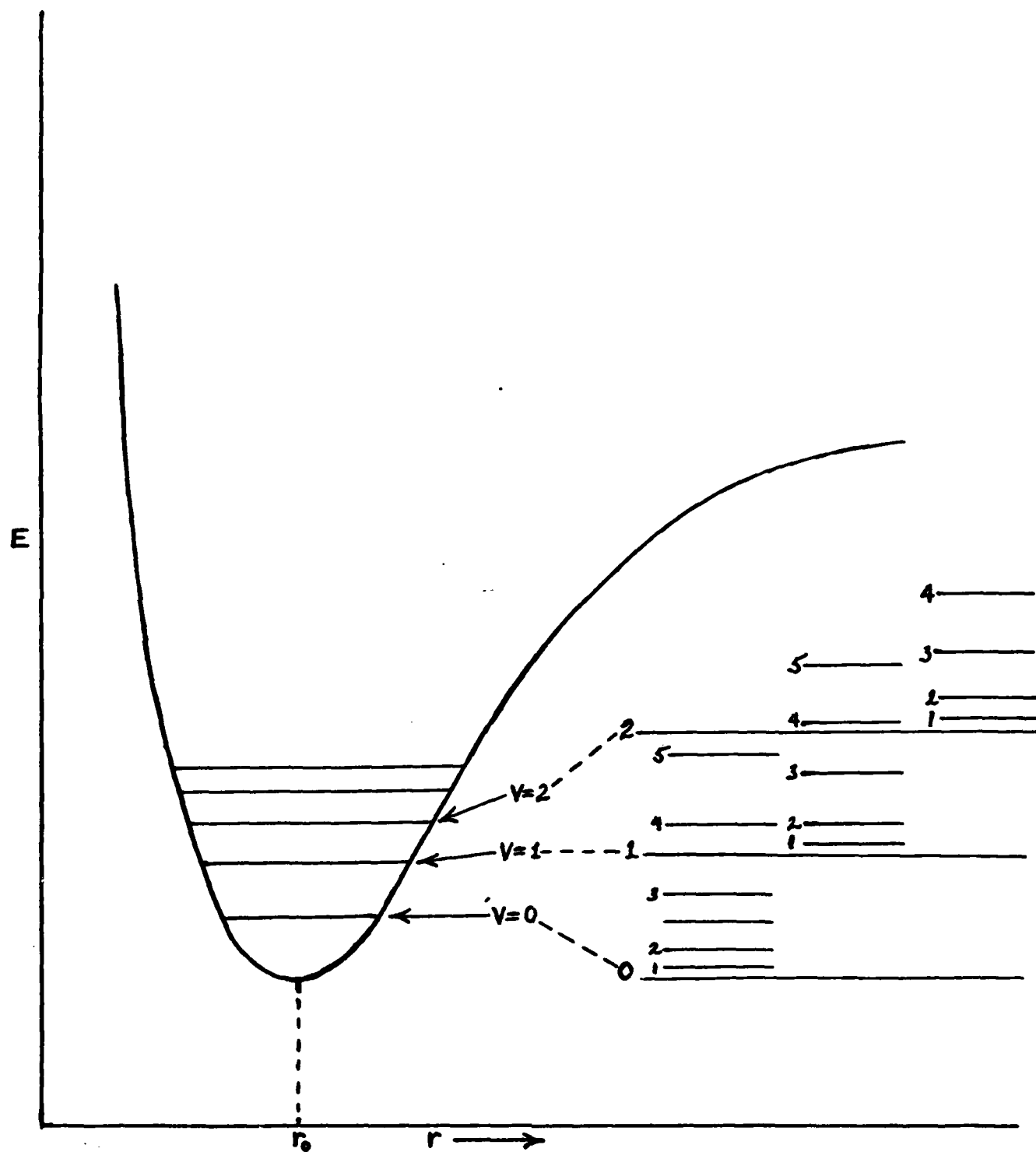


Figure 1 Energy Level Diagram for HF

broadening is the result of energy damping or decay, which diminishes as

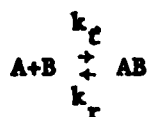
$$e^{-t/2\tau_R} \quad [11:133]$$

where τ_R is the decay lifetime. The line width is then $1/\tau_R$ or $\Delta\omega_R = 1/\tau_R$ [12], [19:100].

Collisional broadening is the result of collisions of the activated species with other molecules present [18:339]. Such collisions are generally elastic and thus no energy transfer occurs. The result is a brief interruption of emission or absorption by the activated molecule.

Kinetics Model for HF

The equilibrium between reactants and products can be shown by the equation



The activation energy, A^+ and ionization energy are shown below

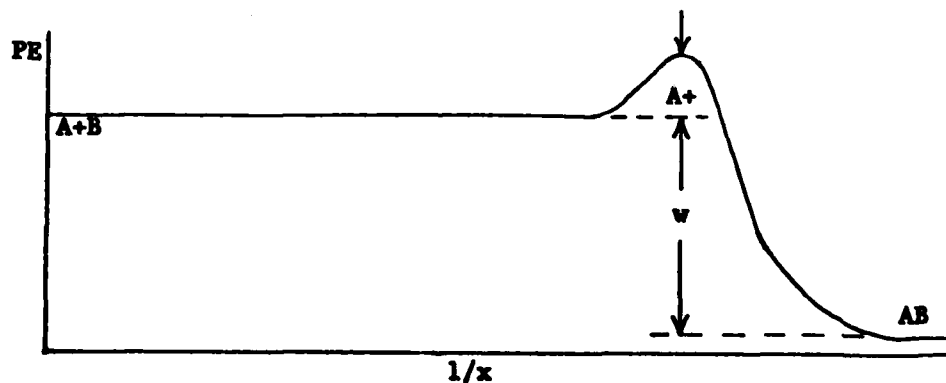


Figure 2 - Potential Energy for $A+B \rightarrow AB$

$$k_t = n_A n_B V \sigma_{AB} e^{-A^+/kT}$$

$$k_r = n_{AB} e^{-(w+A^+)/kT}$$

n_A, n_B, n_{AB} are the concentrations of A, B and AB respectively.

V is the relative velocity between A and B

σ_{AB} is the cross section [9:8-9]

This scheme can be extended to reactions of the form



The vibrational energy state of AB may be exceeded by many times by the reaction energy, w . Energy from w which does not show up in vibration goes into translational and rotational moles.

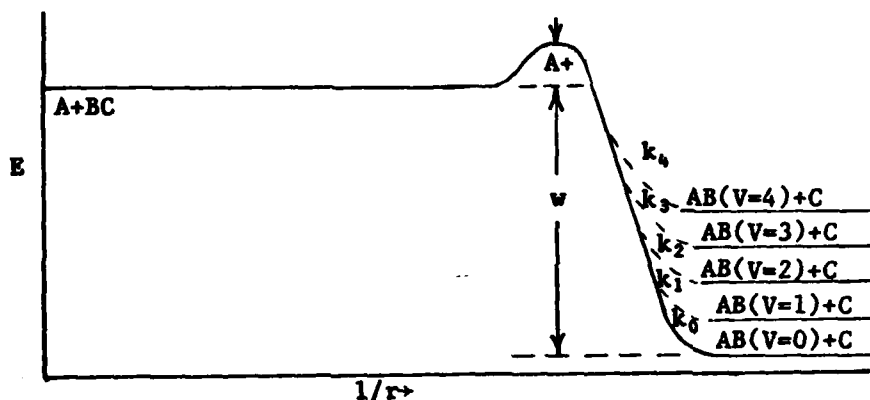


Figure 3 - Potential Energy Diagram for $A+BC \rightarrow AB+C$

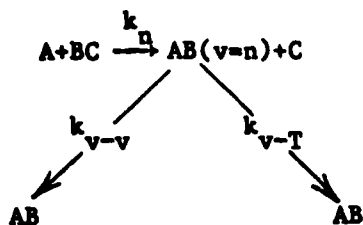
The forward reaction rate constant can be written as

$$k_f = \sum_i k_i$$



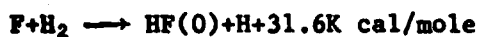
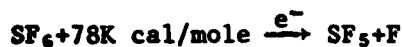
Then k_f is the sum of rate constant producing molecule AB in the various vibrational states.

Typically A is an atom and BC is a molecule. If the relaxation is collision dominated and k_{v-v} is the vibrational relaxation rate, [9:28-29].

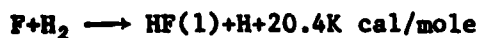


and k_{v-T} is the relaxation rate for V-T processes, the above equation gives the competing processes.

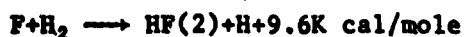
This model can be used to describe the pump laser used in this investigation. The pump laser is a Lumonics TEA 212 series HF chemical laser operating by the method of transverse excitation of the lasing gas mixture (SF_6 , H_2 , He and O_2). This method allows a large amount of energy to be introduced into the gas at pressures of 60 to 70 torr and at voltages of 60 to 70 KV. The gases are exposed to large current densities and the energy of the electrons in the discharge is sufficient to dissociate some of the SF_6 molecules. The F atoms formed are then reacted with H_2 . These form HF molecules in vibrationally excited states (HF*). Relaxation by vibrational-rotational transition to the next lower vibrational band results in lasing [23:7]. The (cold) reaction is as follows:



$$k_0 = 1.2 \times 10^{13} \times 10^{-(350/T)} \text{ cm}^3/\text{mole-sec}$$



$$k_1 = 2.4 \times 10^{13} \times 10^{-(350/T)} \text{ cm}^3/\text{mole-sec}$$



$$k_2 = 8.2 \times 10^{13} \times 10^{-(350/T)} \text{ cm}^3/\text{mole-sec}$$



$$k_3 = 4.1 \times 10^{13} \times 10^{-(350/T)} \text{ cm}^3/\text{mole-sec}$$

[26:11].

(see figure 4)

As rotational relaxation is very rapid compared to v-v and v-T, molecules in a given vibrational state will soon be partitioned into a Boltzman distribution by collisions [24:13]. As expected, the only lines seen are P branch lines ($\Delta J = +1$) in $v=1 \rightarrow v=0$, $v=2 \rightarrow v=1$ and $v=3 \rightarrow v=2$ [23:7].

The SF_6 is very stable and can be made to react only under very extreme circumstances [20:12-13]. The laser uses a 60KV electric discharge to obtain F from SF_6 .

As mentioned earlier, the harmonic oscillator is a reasonable approximation of the anharmonic oscillator for small vibrational numbers, and if this is accepted, the qualitative features of a colliding system pumped by a laser can be predicted.

Using the simplest case where only the first excited state ($v=1$) of HF is pumped by the laser, three possibilities exist:

(1) A weak laser pulse leads to a small population of the excited state. V-V relaxation can be neglected since an excited HF molecule undergoing V-V exchange with another HF molecule will not alter the physical state of the gas. Therefore the observable relaxation mechanism is V-T by thermalization.

(2) A strong pulse of short duration ($\tau_{\text{FWHM}} < \tau_{\text{V-T}}$) creates a very large excited state population. Now $\text{HF}^* - \text{HF}^*$ collisions are important and through such collisions some molecules will reach $v=2$ by

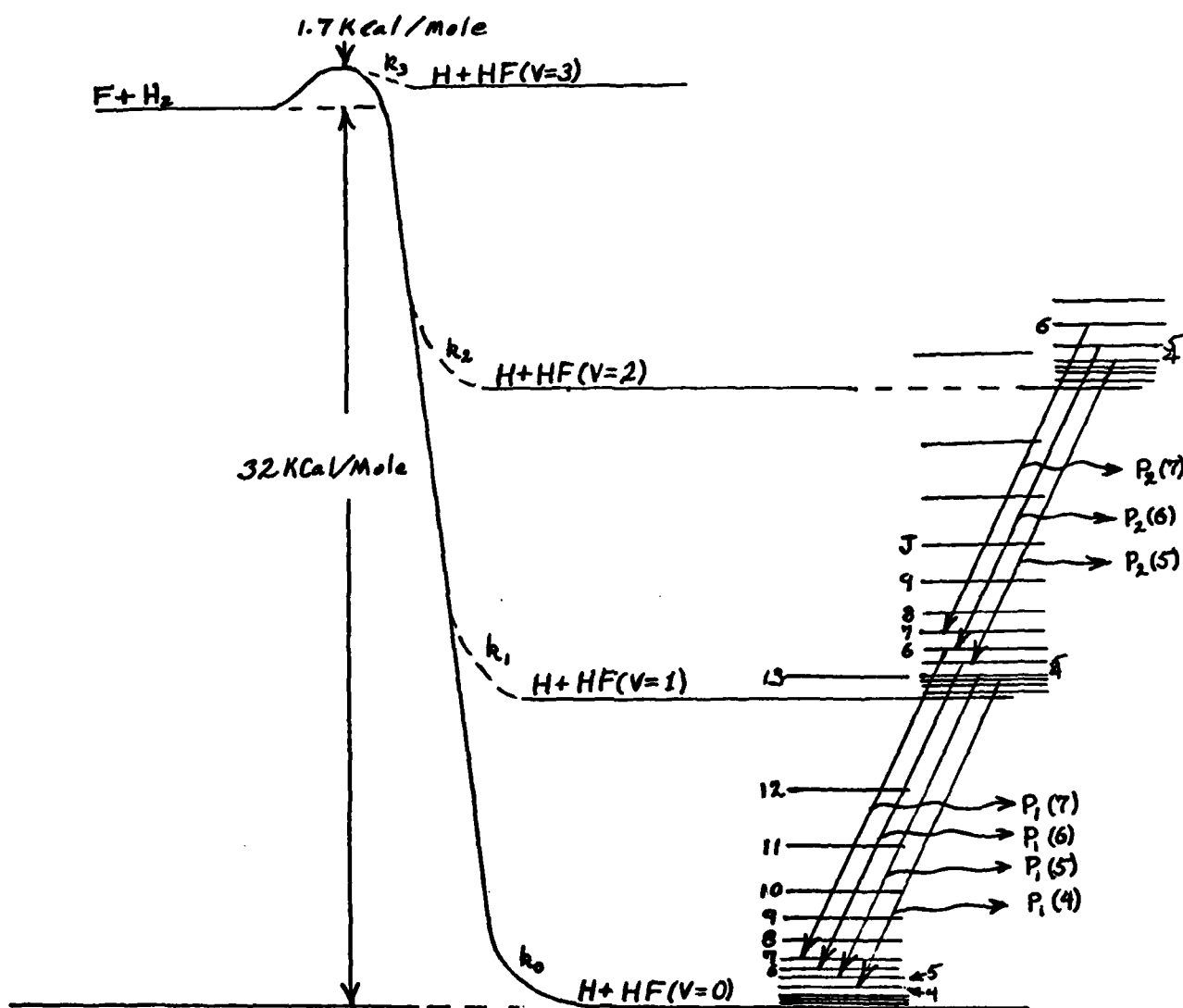
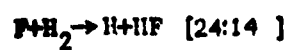


Figure 4 Potential Energy Diagram for

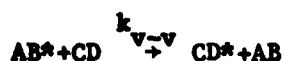


v-v exchange. Depletion of the first excited level will result from population of higher levels.

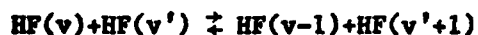
(3) A strong pulse of long duration ($\tau_{v-v} < \tau_{FWHM} < \tau_{v-T}$) creates a very high excited first state. Energy can accumulate in high vibrational states as depletion of the first excited level is balanced by absorption. The level pumped by the laser is depleted via v-v collisions with highly excited molecules. The ground state is replenished and absorption increases. The gas becomes like a saturable absorber with shorter relaxation times as populations of highly excited levels grow. Thermal heating does not affect the system for $\tau_{FWHM} < \tau_{v-T}$. The HF/He mixture should be more immune to heating than pure HF due to the buffer effect of He gas [25:102-104].

The HF ORTL uses the pump laser described previously to pump optically a second medium, in this case an HF/He gas mixture. The result is an optically resonance pumped HF gain medium where HF molecules are excited by an external multiline pulsed HF laser beam. The absorbed energy is redistributed among the vibrational levels [5:24].

The energy redistribution of interest in the pulsed ORTL is the v-v exchange described by



specifically, in the ORTL cell (figure 5) exchanges are of the form



The rates for vibrational-vibrational energy transfer can be very fast for nearly resonant collisions described by the above equation. The vibrational-vibrational process can cause rapid relaxation of a non-Boltzman vibrational distribution into a Boltzman distribution.

Relaxation rates for vibrational-vibrational exchange are often much faster (orders of magnitude when $\bar{\omega}_e$ is large) than vibrational-translational rates. If the pump rate is much faster than the vibrational-translational rate, the system rapidly approaches a vibrational energy which is much higher than the translational energy for times short compared to τ_{v-v} . Then a partial population inversion may exist [9:60].

The spectrum of an HF multiline laser interacting with an HF/He gas is too complex to be discussed in a straightforward manner. Considerable computational effort would be required to take into account the details of the exciting laser and the influence of the relaxation rates. A reasonable understanding can be gained by use of a simpler model. The model consists of an energy system with a ground state and a first vibrational level and the attendant rotational levels. A pulsed pump frequency $F(J)$ is introduced which incites resonant transitions from level $v=0, J$ to level $v=1, J-1$. The system is no longer in equilibrium and now thermalizes via inelastic collisions. Relaxation occurs by V-T, V-V, R-T processes and their effect is determined in part by their relative temporal characteristics:

$$\tau_{V-T} \gg \tau_{V-V} \gg \tau_{R-T}$$

A molecule which undergoes a transition to a higher vibrational level tends to remain in that level as the V-V relaxation rate is long compared to R-T relaxation times. The fast R-T relaxation time

insures it will not stay in the initial rotational level. The rotational distribution of the upper and lower vibrational levels will be approximately Boltzman, yet it is still possible to bleach a single vibrational rotational transition. Then for anytime $t \ll \tau_{V-T}$, the system is in near steady state [21:273-274].

After having absorbed energy from an IR laser pulse, some of the molecules remain in vibrationally excited states. Thermalization may occur through two channels if inelastic collision rates are high enough. In V-V,R relaxation the total number of quanta is conserved though both partners in the collision change their vibrational numbers.

$$HF(V)+HF(V') \rightleftharpoons HF(V-1)+HF(V'+1)$$

Any losses are accounted for by the rotational or translational mode. In V-R,T relaxation [25:102-103].

$$HF(V)+HF(V') \rightleftharpoons HF(V-\Delta V)+HF(V')+\Delta E(V,\Delta V)$$

where ΔV is the number of quanta transferred to R-T energy [21:62-63].

Energy transfer to or from rotation and translation destroy or generate vibrational quanta.

Vibrational levels well above those pumped by the laser can be populated for a certain time though the system ends up in thermal equilibrium. This is possible so long as $E_v \gg kT$ and because V-V processes as a rule are much faster than V-T processes. Then prior to V-T relaxation, energy coupled into a vibrational mode of the molecule redistributor over the vibrational states [25:103].

The rate coefficient for the reaction



is $k = 1.5 \times 10^{12} \text{ T}^{\frac{1}{2}} \text{ cm}^3 / \text{mole-sec}$ [5:11]. The rate equations for V-V reactions are

$$\frac{dN_1}{dt} = -N_1 N_0 \sigma v - 2N_1 N_1 \Sigma v + 2N_0 N_2 \Sigma v$$

$$\frac{dN_2}{dt} = -N_2 N_0 \sigma' v - N_0 N_2 \Sigma v + N_1 N_1 \Sigma v$$

where v = molecular RMS velocity

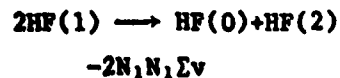
$N_0, 1, 2$ are the populations in the ground, first and second vibrational states, respectively.

Σ is the V-V energy transfer cross section for the above reaction.

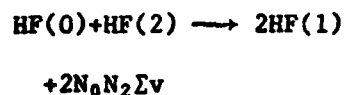
σ, σ' are the cross sections for V-T (or V-R) energy transfer for $V=1$ and $V=2$ respectively

[27:470].

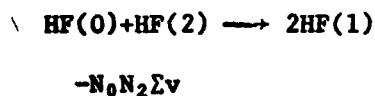
The V-V reactions contribute to the rate equations as follows:



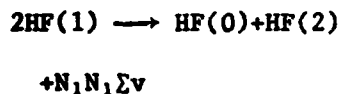
as two N_1 are lost to level one. One to level two and one to the ground state



as N_0 and N_2 are gained to level one. One from the ground state and one from level two. The above two reactions are competing processes.

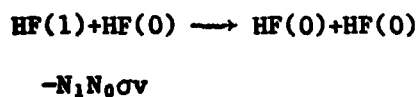


as N_2 is lost from level two, and along with N_0 , is gained by level one.

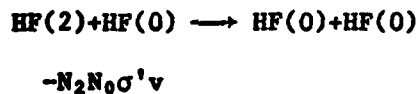


as N_1 is gained from level one. The ground state receives the other (equal) quarter of energy.

V-R and V-T reactions account for the remaining losses from levels one and two by



as N_1 is lost from level one to the ground state -



as N_2 is lost from level two to the ground state.

It should be pointed out here that HO model previously assumed predicts $\Delta V=1$ and for $\Delta V>1$ transitions to be negligible compared to $\Delta V=1$ transitions. HF, however, is far from an ideal harmonic oscillator and at this point the HO model begins to fail 22:62-63 .

The initial conditions for the rate equations are $N_1=N_1^0$, $N_2=0$. Rotational relaxation is assumed to be much faster than vibrational relaxation [27:470], [24:7-8].

The rate equations are coupled, nonlinear, inhomogeneous differential equations. The solution can be simply obtained by noting that for any given time $N_2 \ll N_1 \ll N_0$. The equation can now be linearized and an approximate result obtained. Let

$$\frac{dN_1}{dt} \approx -N_1 N_0 \sigma v$$

as $N_0 N_1 \gg N_1 N_1$ and $N_0 N_1 \gg N_0 N_2$.

then

$$\frac{dN_1}{N_1} \approx -N_0 \sigma v dt$$

$$\ln N_1 - N_0 \sigma v t + \ln C_0$$

$$N_1 \approx C_0 \exp(-N_0 \sigma v t)$$

$$\text{at } t=0 \quad N_1 = C_0 = N_1^0$$

$$\text{and } N_1 = N_1^0 \exp(-N_0 \sigma v t)$$

$$\frac{dN_2}{dt} = -N_2 N_0 v \sigma' - N_2 N_0 \Sigma v + N_1 N_1 \Sigma v$$

$$= -N_2 N_0 v (\sigma' + \Sigma) + (N_1^0)^2 \exp(-2N_0 \sigma v t) \Sigma v$$

[27:470]

using the form for a linear differential equation

$$\frac{dy}{dx} - p(x)y = Q(x)$$

let $\mu = e^{\int p(x) dx}$ be an integrating factor

such that

$$\frac{d}{dx}(\mu y) = \mu Q$$

with solutions of the form

$$\mu y = \int \mu Q dx + C$$

$$\text{or } y e^{\int p(x) dx} = \int Q e^{\int p(x) dx} dx + C \quad [28:40].$$

now

$$\frac{d}{dt} N_2 \exp \int (\sigma' + \Sigma) N_0 v dt =$$

$$(N_1^0)^2 \exp(-2N_0 \sigma v t) \exp \int (\sigma' + \Sigma) N_0 v dt$$

$$N_2 \exp \int (\sigma' + \Sigma) N_0 v dt =$$

$$(N_1^0)^2 \exp(-2N_0 \sigma v t) \Sigma v \exp \int (\sigma' + \Sigma) N_0 v dt dt$$

$$N_2 \exp \int (\sigma' + \Sigma) N_0 v dt =$$

$$(N_1^0)^2 \Sigma v \int \exp\{N_0 v (\sigma' + \Sigma) - 2\sigma t\} dt$$

=

$$\frac{(N_1^0)^2 \Sigma v \exp\{N_0 v (\sigma' + \Sigma) - 2\sigma t\}}{N_0 v (\sigma' + \Sigma) - 2\sigma} + C_1$$

$$N_2 = \frac{(N_1^0)^2 \Sigma v \exp(-2\sigma v t)}{N_0 v (\sigma' + \Sigma) - 2\sigma} + C_1 \exp -(\sigma' + \Sigma) N_0 v t$$

at $t=0$

$$N_2^0 = \frac{N_1^0 \Sigma}{N_0 (\sigma' + \Sigma) - 2\sigma} + C_1 = 0$$

and

$$\begin{aligned} N_2 &= \frac{(N_1^0) \Sigma}{(\Sigma + \sigma' - 2\sigma)} \exp(-2\sigma N_0 v t) - \exp -(\sigma' + \Sigma) N_0 v t \\ &= \frac{(N_1^0)^2 \Sigma \exp(-2\sigma N_0 v t)}{(\Sigma + \sigma' - 2\sigma)} \{1 - \exp -(\sigma' + \Sigma - 2\sigma) N_0 v t\} \end{aligned}$$

[27:470].

A model for the rate constants ($k_{v \rightarrow v}$) developed by Schmailzl, et al [29:122] was used in a computer program run on a Sinclair ZX-81 micro-computer. The constants were determined by successive approximation anchoring to data obtained from an Aerospace Corporation report by Kerber and Whittier [26:11]. The results for the rate coefficients are as follows (T=300K):

aerospace results	code results	difference
$2.5980762 \times 10^{13} \text{ cm}^3/\text{mole-sec.}$	$2.5980762 \times 10^{13} \text{ cm}^3/\text{mole-sec}$	anchor
1.2990381×10^{13}	1.280073×10^{13}	0.9986%
$0.64951905 \times 10^{13}$	$0.64622654 \times 10^{13}$	0.507%
$0.32475953 \times 10^{13}$	$0.32877064 \times 10^{13}$	-1.235%

The program is listed in appendix B [29:122], [26:11].

The equation for the rate constant for V-V(HF-HF) transitions is

$$k_{v \rightarrow v-1}^{v'-1 \rightarrow v'} = N(T/300K)(v'v)^X \exp -C|E_v + E_{v'-1} - E_{v+1} - E_{v'1}|$$

$$N = 5.3416051 \times 10^{13} \text{ cm}^3/\text{molecule-second}$$

$$C = 4.307 \times 10^{-3} \text{ cm}$$

$$X = 7.58$$

$$T = 300K.$$

The equation for the rate constant for R-R(HF-HF) transitions is

$$K_{J \rightarrow J-1} = ZN(2J+1) \exp \left(-C \frac{E_{J+1} - E_J}{k_B T} \right)$$

$$C = 1.77$$

$$N = 2.0$$

$$Z = 2.80 \times 10^{12} T^{1/2} \text{ cm}^3/\text{molecule-second}$$

$$k_B = \text{Boltzman's constant}$$

$$[29:122].$$

The equation for the rate constant for V-R,T(HF-HF) transitions is

$$k_{v \rightarrow v-1}^{HF} = v \left(10^{14} T^{-0.8} + 10^{0.4} T^{3.5} \right) \quad [26:11].$$

The second of these equations was the rate constants which were calculated by Schmailzl, et al [23:122].

Jurisch and Crim obtained the following expression for vibrational state populations [30:4456-4457]:

$$N_v = N_v^0 \exp(-k_v n t)$$

$$N_{v-1} = N_v^0 \frac{k_{v,v-1}}{k_v - k_{v-1}} \exp(-k_{v-1} n t) - \exp(k_v n t)$$

$$N_{v-2} = N_v^0 \alpha \exp(-k_{v-2} n t) - \beta \exp(-k_{v-1} n t) + \gamma \exp(-k_v n t)$$

where:

$$\alpha = \frac{k_{v,v-1} k_{v-1,v-2}}{(k_v - k_{v-2})(k_{v-1} - k_{v-2})} + \frac{k_{v,v-2}}{(k_v - k_{v-2})},$$

$$\beta = \frac{k_{v,v-1} k_{v-1,v-2}}{(k_v - k_{v-1})(k_{v-1} - k_{v-2})},$$

$$\gamma = \frac{k_{v,v-1} k_{v-1,v-2}}{(k_v - k_{v-1})(k_v - k_{v-2})} - \frac{k_v}{(k_v - k_{v-2})}$$

v is the vibrational level pumped, N_v^0 is the initial population of level v and n is the number density of the ground state HF molecules. The first two equations show good agreement with those used by Osgood, et al [27:470], [31:254] and the third is accepted for evaluation of three level systems [30:4456-4457].

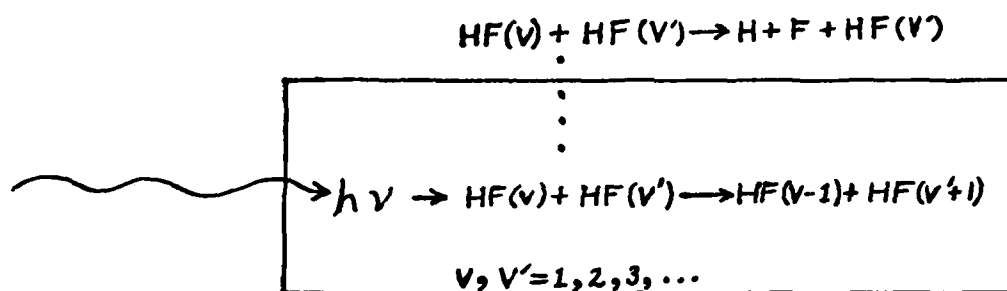


Figure 5 HF V-V), Dissociation Species

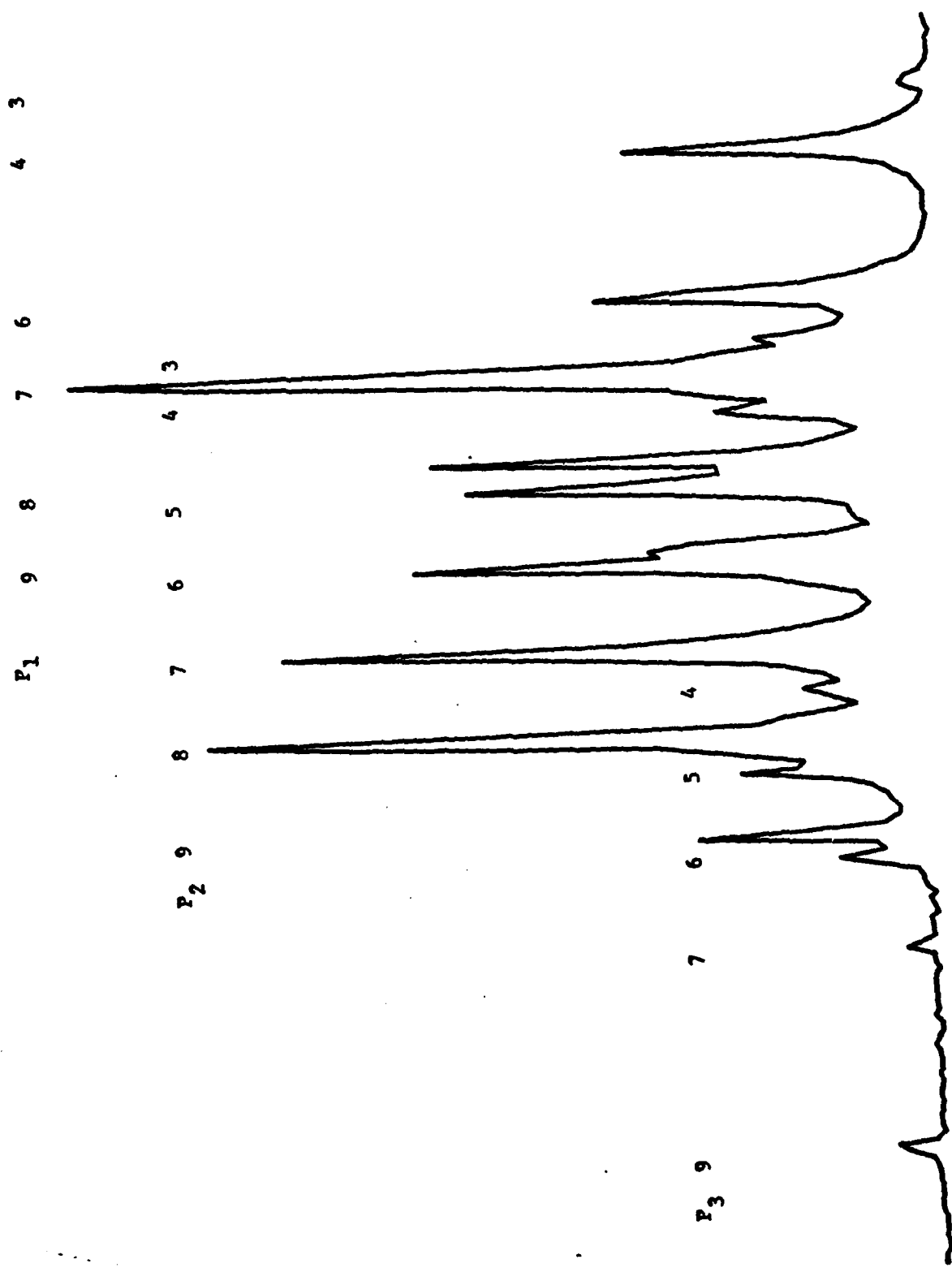


Figure 6 HF Spectra [23:58]

Experiment

This experiment was designed to measure gain and absorption of HF during pumping by the output beam of a pulsed HF laser as a function of temperature and time. The experiment is set up similar to a procedure described by Ashmore and Donovan [34:120]. First the various parts of the ORTL experiment are described, then the HF pump laser output characteristics are reviewed and the energy requirements for the ORTL are discussed. Then finally, the laser operation, safety and alignment procedures are covered.

Gas System

The vacuum system is described to allow an understanding of how the gases can be introduced into the two cells in various arrangements (see figure 7).

The two cells are connected such that the He can be fed into reference cell (F) and HF/He or HF gas into the ORTL cell (G). The cells can then be evacuated and the gas pressure measured by a gauge for each cell. The gas can then be evacuated through a common pump independently for each cell. The cells are also interconnected to permit He flushing of the entire system and simultaneous use of HF gas in both cells. The cells are five centimeters long and 3/8 inch inner diameter and constructed of aluminum. Viton "O" rings 1/4" inner diameter are used on the ends with 4mm thick one inch diameter CaF_2 windows. Aluminum tubing is used throughout the system except for the

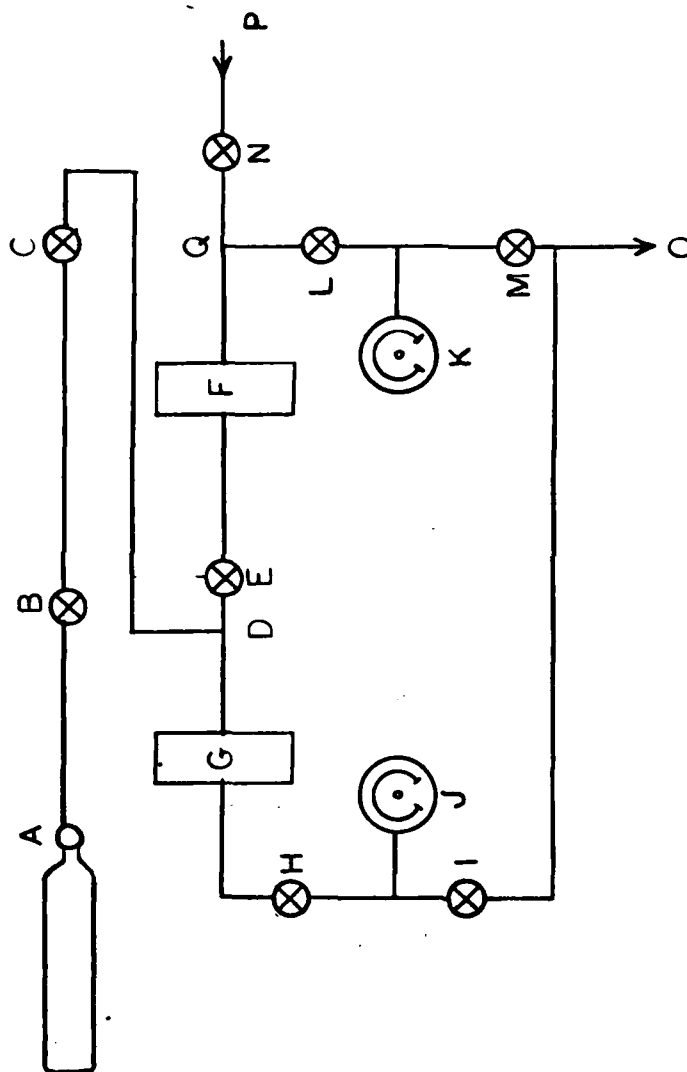


Figure 7 Gas System

helium line and to the exhaust pump (where contamination is of no concern) where plastic tubing is used. Aluminum was selected due to cost and availability advantages over monel metal. The aluminum will quickly passivate in the presence of concentrated HF gas and then no further deterioration should result. Monel metal fittings and valves were used when possible (5 bellows valves). The monel metal needle valves were installed in the system where critical adjustments to pressure were needed. Two of these valves failed and the third leaked and had to be replaced. All three needle valves were replaced by stainless steel which should function well with the HF/He gas but will have a limited life with the HF gas (as will the pressure gauges which will have to undergo continual recalibration for use in an HF environment).

The He feed (see figure 7) to the reference cell is controlled by a stainless steel needle valve (N) and a brass bellows valve (P). The needle valve is connected in a "T" (Q) with a monel bellows valve (L) leading to the He pressure gauge (K), followed by a second bellows (M) then the vacuum line (O). A monel bellows (E) connects the two cells along with a "T" (D) to a stainless steel needle valve (C) and a monel bellows valve (B) to the HF/He or HF gas (A). The other end of the ORTL cell (G) is connected by a monel bellows (H) to a pressure gauge (J) followed by a stainless steel needle valve (I), then to the vacuum line (O). The vacuum pump exhausts the gases into the exhaust line used by the Lumonics laser and uses a common scrubber.

Optical Train

The optical path is reviewed in order to give an understanding of the path manipulations required to obtain three different beams from the pump laser (see figure 8).

The output beam is passed through two $\frac{1}{4}$ " apertures (A) used to define the plane into the Lumonics laser and to limit stray radiations. The beam then passes through a calcium fluoride flat rotated 45° about its vertical axis (B), which acts as a beam splitter.

The reflected portion of the beam is the reference beam and is directed through the reference cell (R). The beam is now reflected from two turning flats (S,T) through a step ladder mirror assembly (U) and reflected off another calcium fluoride flat (N) at 45° about its vertical axes. The beam is now directed into the spectrometer.

The transmitted portion of the beam from the first calcium fluoride flat (B) is directed into a silicon wafer (C) rotated 45° about its horizontal axis (see figure 9).

The beam transmitted through the silicon wafer (C) will remain vertically polarized and is reflected off three turning flats (D,E) in a step ladder arrangement and through a zinc selenide flat (F) rotated at Brewster's angle about its horizontal axis then into the ORTL cell (I). This beam retains 92.2% of its energy and is used as the pump beam (see analysis in the HF Pump Laser section of this chapter).

The beam reflected from the silicon wafer (C) (see figure 9) is reflected from a parallel mirror (G) to a second mirror (H) which directs the beam onto the zinc selenide flat (F). The beam is then reflected at Brewster's angle into the ORTL cell (I). The beam is rotated by approximately 45° and is now at 0.25% of its original energy.

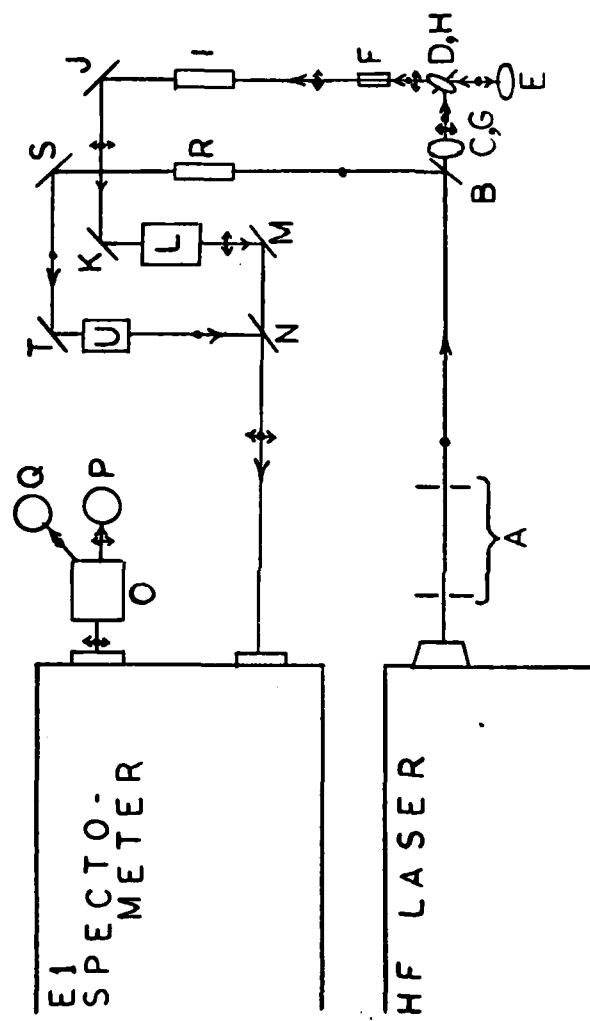


Figure 8 Optical Train

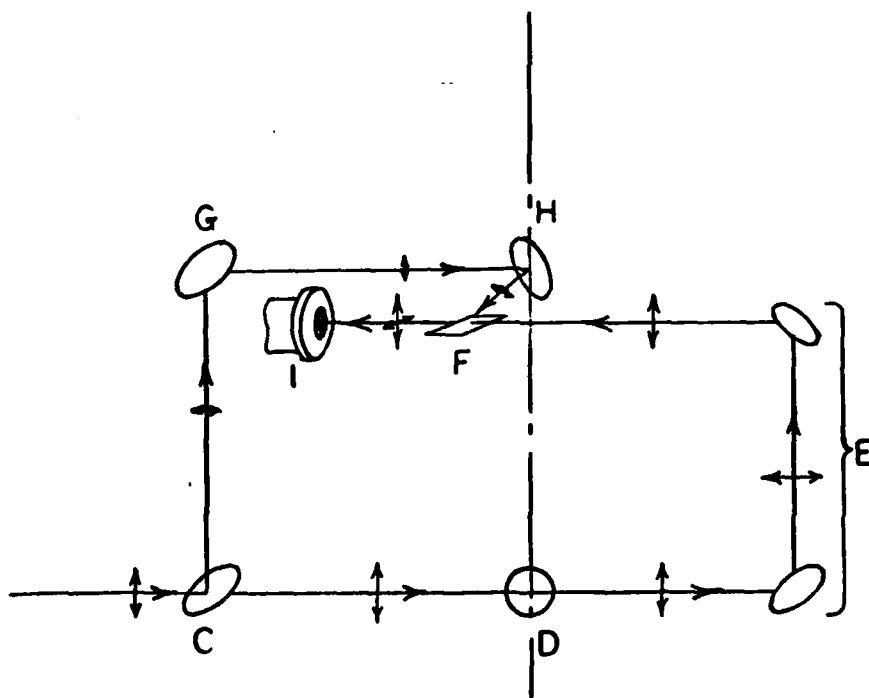
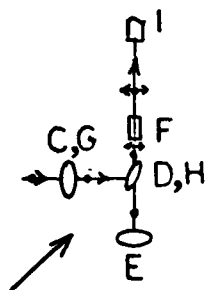


Figure 9 Pump/Probe Train Detail

This beam is used as a probe beam and only the horizontal component is preserved.

The recombined beam now passes through the ORTL cell and is reflected off a pair of turning flats (J,K). The beam now strikes a zinc selenide flat at Brewster's angle (L) where only the horizontal component is reflected. The vertical component (pump) is absorbed in a wooden block. The horizontal component (probe) is reflected again off a mirror parallel to the zinc selenide plate, then off a turning flat (M) and through the second calcium fluoride flat (N) into the spectrometer.

The output from the spectrometer meets two zinc selenide plates at Brewster's angle (O), the first beam is rotated about its horizontal axis and in parallel with a mirror. The second beam is rotated about its vertical axis. These serve to separate the two polarizations: the horizontal is the probe and the vertical is the reference. The beams are now detected at P and Q.

Electronics

This section describes methods used to detect and process the signals from the ORTL and reference cells after line selection by the spectrometer.

Two IR detectors were used: an InSb detector (Santa Barbara) and a HgCd Te detector (S.A.T.). The InSb detector was used to detect the probe signal from the ORTL cell and the HgCd Te detector was used to detect the reference signal. Both detectors require approximately 15 VDC from separate external power supplies so as to reduce cross talk. The signals were amplified before they entered the boxcar averager. The boxcar averager has the options of averaging channels

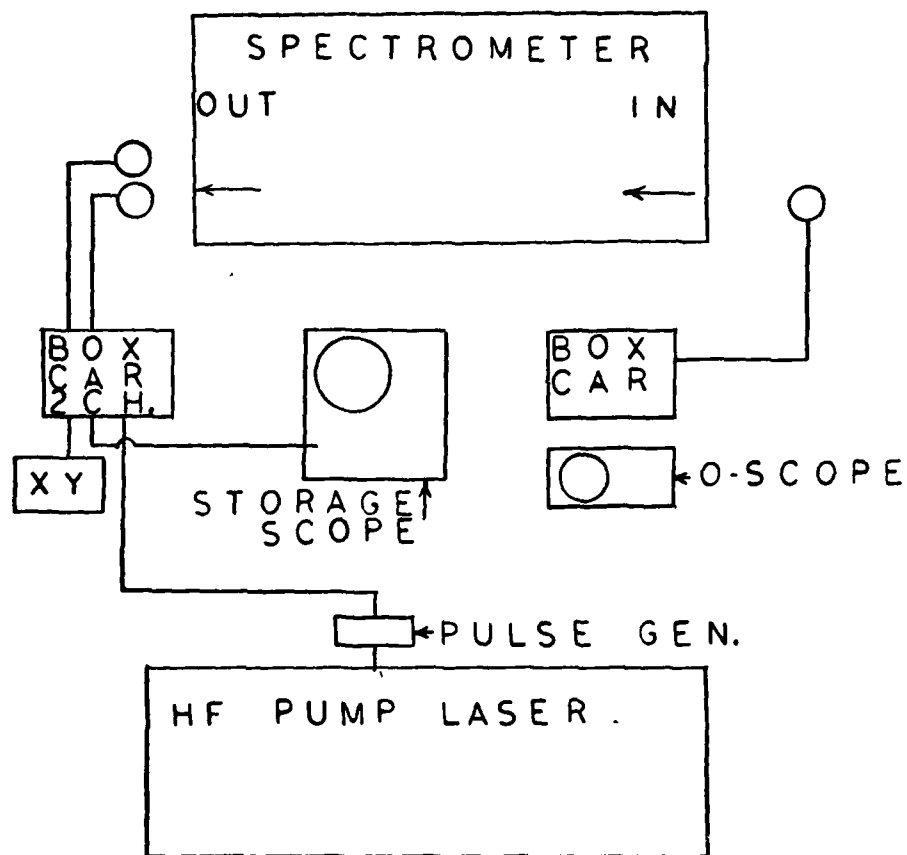


Figure 10 Electronics

A (probe) or B (reference) or $A/|B|$ or $\log(|A|/|B|)$. An average was taken over 10 to 25 pulses and the output was plotted on an X-Y plotter [35:II-6]. The input pulse could be monitored on a storage oscilloscope. The signal to noise ratio required was $\sim 1000/1$ for optimum performance of the boxcar averager [36]. The pump laser generates very large electromagnetic pulses from the 60 KV on the electrodes. The noise resultant at the input of the boxcar averager can be as large as the signal for small slit widths of the spectrometer. Much of the noise can be averaged out in the signal processing using $\log(|A|/|B|)$ but the uncertainties generated by such a large noise component warrant the use of Faraday cages for the detectors and boxcar averager, connecting the detectors to the boxcar by triaxial cable. One such cage was designed to house the boxcar averager and oscilloscope and the frame was built. The required copper mesh could not be obtained through the procurement cycle in time to complete this experiment. A listing and description of the equipment used in this investigation can be found in Appendix C.

The problem with noise was so severe that the electromagnetic pulse from the Lumonics laser was sufficient to cause the X-Y plotter pen to jump. This was verified by disconnecting that unit from other circuitry. The jumping occurred only when the plotter was turned on thus eliminating vibration as a source of the jump. The two detectors used in the investigation, though similar in response characteristics, differed in their response to noise. This difference proved too great to use the detectors in an A/B or $\log A/B$ arrangement.

The experimental setup was reduced to a single path through the ORTL cell (I) (see figure 8) to detector P. The detector Q and

Brewster's windows (O) were removed from the path. A further change in the system included the use of a chopper to block alternate pulses of the pump beam. The TTL logic on the EG&G 1653 [39:IV-2] was used to select channel A to receive the signal from the probe pulse with the pump and channel B to receive the signal from the probe pulse without the pump. A separate collection of data was required for helium in the cell. A second chopper was installed after removing the pump chopper. This chopper blocked alternate pulses from the probe. This tested for presence of the pump pulse in the probe signal due to slight inaccuracies in the angle of the pump filter (L) (see figure 8). The first chopper was located between elements C and D (see figure 9) and the second chopper between elements G and H.

ORTL Experiment

The output of the Lumonics laser was originally intended to be compressed to $\frac{1}{4}$ inch by a telescope, however, the unstable resonator could not be aligned to produce a collimated beam (see section on safety and alignment), therefore, the laser output was used as multi-line, multi-mode with a hot spot and a beam divergence approximately 0.0012 radians. Reducing the KV on the laser reduces the intensity of the hot spot. The $\frac{1}{4}$ " apertures should together with the cells controlled beam spread over the two meter path length.

The advantage of using a reference cell simultaneously with the ORTL cell lies in the $\log(I_A/I_B)$ reduction of the boxcar averager [35:II-6]. The same pulse was used to obtain both A and B, thus variations from pulse to pulse in intensity were averaged out.

HF Pump Laser

The HF pump laser (Lumonics TEA-212) incorporates an unstable resonator in its optical design. Properly aligned, the resonator produces single mode, multi-line lasing in the 2.6 micrometer to 3.1 micrometer range. A spectrum of the output is shown in figure 6. For HF operation, the lines scan are shown in table I.

Table I - HF Laser Lines

<u>Vibrational</u>	<u>Rotational</u>	<u>Wavelength</u> (micro-meters)
v=1→v=0	P(3)	2.608
	P(4)	2.690
	P(5)	2.673
	P(6)	2.707
	P(7)	2.744
	P(8)	2.783
	P(9)	2.823
	P(3)	2.727
	P(4)	2.760
v=2→v=1	P(5)	2.795
	P(6)	2.832
	P(7)	2.871
	P(8)	2.911
	P(9)	2.954
	P(3)	2.854
	P(4)	2.889
	P(5)	2.926
	P(6)	2.964
v=3→v=2	P(7)	3.005
	P(8)	3.048
	P(9)	3.093

Oscilloscope traces of the laser output with the unstable resonator are shown in Appendix A. Pulse duration is 500 nsec FWHM [23:58]. Operating instructions for the Lumonics laser are listed in Appendix A.

An estimate of the power required to pump the HF/He gas in the ORTL cell is necessary. If a pressure of 50 torr of HF/He gas mixture is used in the ORTL cell, then at 1% HF by volume, the effective HF

pressure is = 0.25 torr

$$= 333.224 \text{ dynes/cm}^2.$$

The volume of the ORTL cell is 3.563 cm^3

Then using the ideal gas equation of state

$$PV = NkT$$

N is found to be 2.92×10^{16} , the number of HF molecules present in the ORTL cell at 295K. If it is assumed that one photon in three will pump an HF molecule [36], then to pump the HF population completely, the required number of photons is approximately $3N$ or 8.75×10^{16} photons.

Based on a discussion presented in Appendix G, it was assumed that the number of photons is $n=3N$. Then the power required of the laser is

$$p = nh\nu/\tau_c$$

where n = number of photons

$$h = 6.626 \times 10^{-34} \text{ Joule-sec}$$

$$\nu = 1.079 \times 10^{14} \text{ Hz (from } \lambda = 2.78 \text{ micrometers)}$$

$$\text{and } 1/\tau_c = \frac{c}{n_o L} \left[2\alpha_o L + \ell n \frac{1}{R_1 R_2} \right]$$

$$\text{where } c = 3 \times 10^8 \text{ m/sec}$$

$$n_o = \text{index of refraction of gases in pump laser} \approx 1.001$$

$$L = 1 \text{ meter}$$

$$R_1 = R_2 \approx 0.97$$

$$\alpha_o \text{ is assumed small}$$

$$\text{Then } 1/\tau_c \approx 2 \times 10^7 \quad [19:427]$$

and $p = 1.25 \times 10^5$ watts of power required of the Lumonics laser to pump the HF in the ORTL cell. The energy is

$$E = p\tau$$

where τ is the pulse duration at FWHM, which is 500 nsec. Then
 $E = 0.0625$ Joules.

The Lumonics nominally provides $\frac{1}{2}$ Joule per pulse of energy. The attenuation in the optical train reduces the available energy in the pump beam by about eight percent.

The beam out of the Lumonics appears to contain only the vertical component of polarization. This was determined by reflecting the beam off a silicon wafer at Brewster's angle with the wafer rotated about its vertical axis. Very little energy passed through the wafer but a large component was reflected (determined by qualitative measurements using thermal paper to detect beam location and to some extent, its intensity). There is apparently little if any horizontal component of polarization present in the beam.

The present optical arrangement directs the pump beam through a calcium fluoride flat at 45° rotated about its vertical axis then transmitting through a silicon wafer at 45° rotated about its horizontal axis, then, transmitting through a zinc selenide flat at Brewster's angle, rotated about its horizontal axis using Fresnel's equations [37:570-573] listed in Appendix D:

These equations are used in a program run on a Sinclair ZX-81 micro-computer. The program is listed in Appendix B.

For the CaF_2 flat at 45° , (assuming vertical polarization only) rotated about the vertical axis (// implies the polarization is parallel to this axis of rotation)

$$R// = 0.073$$

$$T// = 0.927$$

Then 92.7% of the pump beam is transmitted and 7.3% is reflected to the reference cell (see optical description earlier in this chapter). The beam now strikes the Si wafer at 45° rotation about its horizontal axis (\perp implies the polarization is normal to thin axis of rotation)

$$R_{\perp} = 0.0054$$

$$T_{\perp} = 0.9946$$

Then 99.46% of the 92.7% or 92.2% of the pump beam is transmitted and 0.5% is reflected (this portion becomes the probe beam). The transmitted or pump beam next encounters a ZnSe flat at Brewster's angle rotated about its horizontal axis

$$R_{\perp} \approx 0$$

$$T_{\perp} \approx 1$$

Thus the pump beam is at 92.2% of its original strength or 0.461 Joule. The probe is rotated by 45° and reflected off the ZnSe flat at Brewster's angle into the ORTL cell where only the horizontal component of polarization is of interest,

$$R_{//} = 0.504$$

$$T_{//} = 0.495$$

and is $(0.0054)(0.504)(.927) = 0.00252$ or 0.252% of the original beam or 0.00126 Joule. Then the pump pulse is more than adequate to pump the HF molecules and the probe pulse is small enough to prevent significant pumping by that component (approximately 2% by the above method).

Laser Safety and Alignment

The Lumonics laser employs dangerous (60 KV) voltages (at the current levels used) and toxic as well as explosive gases. The beam out of the laser can cause serious eye damage. Therefore a section

addressing laser safety is necessary. Some of the problems encountered in aligning the laser are also recounted.

The safety factors considered were:

(1) The very high voltages used in the resonator cabinet of the Lumonics. These voltages (60 KV) were applied to large capacitors in the electrode circuit. The capacitors are well insulated with mylar and use plastic standoff plates. The voltages will not be of concern so long as the laser cavity cover is not opened and the safety interlock overridden during operation of the laser.

(2) Two potentially dangerous gases are used in the gas supply: Hydrogen and oxygen. Start up and shutdown procedures outlined in Appendix A are designed to insure against concentrations of these gases forming in any location beyond the feed lines. Hydrogen fluoride gas, sulfur dioxide and ozone are the toxic gases produced as reaction by products. These gases are removed from the laser by a pump and vented through sodium hydroxide filters outside the building before venting to the atmosphere. The room in which the experiment took place has an exhaust fan to cope with any possible leakage of gases.

(3) The safe eye exposure distance (SEED) is calculated by

$$SEED = \sqrt{\frac{2E_p}{\pi\theta_{\frac{1}{2}}MPE}} \quad [38]$$

where $E_p = 500\text{mJ}$

$\theta_{\frac{1}{2}} = 12\text{mrad}$

$MPE = 10^{-7}\text{J/cm}^2$

Then the SEED is 16,287 meters. This, of course, is well beyond any reasonable distance in the laboratory. Eye safety goggle densities may

be computed by

$$D = \log_{10} \frac{E_o}{E_p} = 7.1 \quad [38]$$

$$E_p \approx 4 \times 10^{-8} \text{ Joules}$$

Safety goggles with a density of $D=9$ at 2.8 micrometers were available. For an aligned system, no large stray radiations exist and these goggles provide adequate safety so long as the direct beam is not viewed [38].

Alignment Procedures for the Optical Train

A helium neon (HeNe) laser was mounted so as to provide a beam through the spectrometer in reverse then back through the train to the Lumonics. In this procedure the detectors cannot be aligned to the system, nor could the Lumonics be finely aligned. In the final alignment procedure, a strong HF line was selected on the spectrometer P_1 (8)). The Lumonics was set to run at 2 Hz. The signals from the detectors were run into the storage oscilloscope, with the scope triggered by the Lumonics through a pulse generator. The slit width on the spectrometer were set at 1000 micrometers initially for large signal input. Once triggering was established, a detector was placed in the beam path to determine proper operation and beam appearance. The detector was then mounted in position at the spectrometer output and the optics fine tuned to maximize output at the smallest possible entrance slit. The smallest slit attainable was 50 micrometers.

The alignment of the Lumonics is affected by adjustment to the rear grating and the front elements of the unstable resonator. The grating is adjusted by a micrometer and the front setting by opposed

axis controls. Full alignment was not possible with these controls indicating some possible damage to the resonator optics.

Results and Conclusions

The results of the experiments described in the previous section are now presented and compared to the theory presented in the second chapter. Conclusions concerning the ORTL are drawn. Finally, a summary of the investigation, results, and conclusions is presented.

Monochromator Calibration and Line Identification

The identification of the lines used in the ORTL experiment required that the accuracy of the Perkin-Elmer E-1 monochromator be verified. The monochromator was used in the single pass mode for the entire investigation. A Spectra Physics model 133 Helium Neon Laser was used to align the optical system and calibrate the monochromator. The grating used is #244 usable over 2μ to 4μ . The monochromator was tuned to a very strong line at 500μ slit width and then fine tuned at 100μ slit width. The wavelength recorded was 1.8985μ . Then $\lambda = 1.8985\mu = 3\lambda_0$ where $\lambda_0 = 0.632833\mu$. The known value of λ_0 is 0.6328μ and this value would yield a $3\lambda_0$ of 1.8984μ . The calibration of the monochromator was then established.

The lines on which the Lumonics laser lases are listed in Table I. An attempt was made to identify all of these lines. The lines that could be identified are listed in Table II and the lines that could not be identified are listed in Table III.

Table II

Line	wave length (μ)	minimum slit width visible (μ)
P ₃ (7)	3.0045	150
P ₃ (6)	2.9637	100
P ₃ (5)	2.9250	150
P ₂ (8)	2.9105	75
P ₃ (4)	2.8885	200
P ₂ (7)	2.8698	75
P ₂ (6)	2.8312	100
P ₂ (5)	2.7946	150
P ₁ (8)	2.7820	60
P ₁ (7)	2.7435	75
P ₁ (6)	2.7070	150

Table III

Line	Line	Line
P ₃ (9)	P ₃ (3)	P ₂ (3)
P ₃ (8)	P ₁ (9)	P ₁ (5)
P ₂ (9)	P ₂ (4)	P ₁ (4)

The single greatest contributor to the inability to tune the lines listed in Table III is the very serious noise problem mentioned in Chapter III. Some lines may have been too close together to be resolved such as P₂(9) and P₃(6), P₂(6) and P₁(9), P₂(4) or P₂(3) and P₁(7). The inability to properly align the Lumonics laser due to electrode and resonator problems leaves open to question the relative intensities to be expected from the Lumonics laser on these lines.

The lines of interest in Table II are those identified in previous work at AFWL [6]. The pulse shapes of these lines reported by Dr. Drummond are shown in figure 11 [6]. Plots of these lines were also obtained in this investigation. These plots are not true pulse shapes but are instead statistical averages over the pulse duration (figure 12). An aperture delay range of 1 microsecond and an aperture duration of 200 nsec were used. An explanation of settings for the boxcar averager

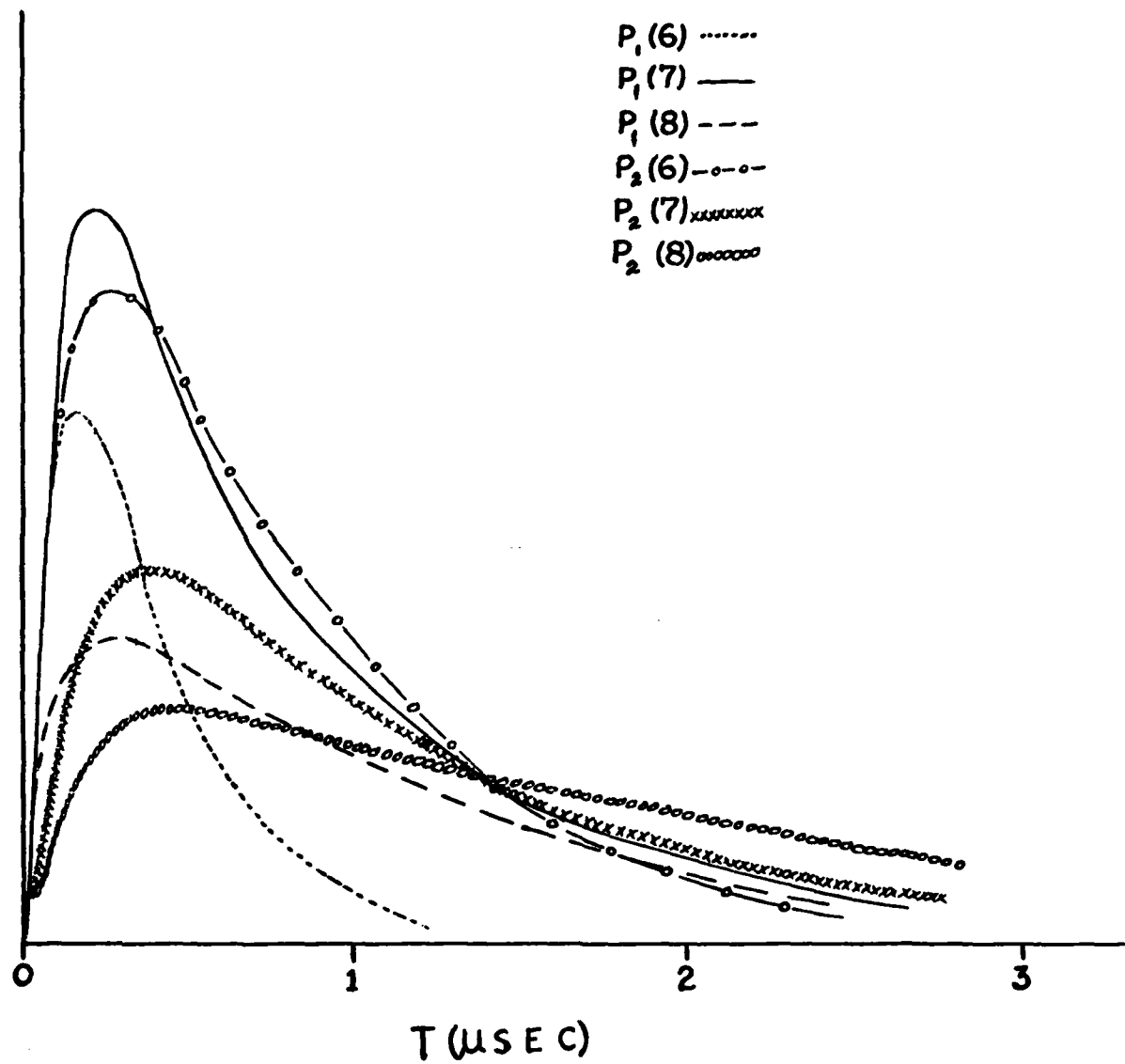


Figure 11 [6]

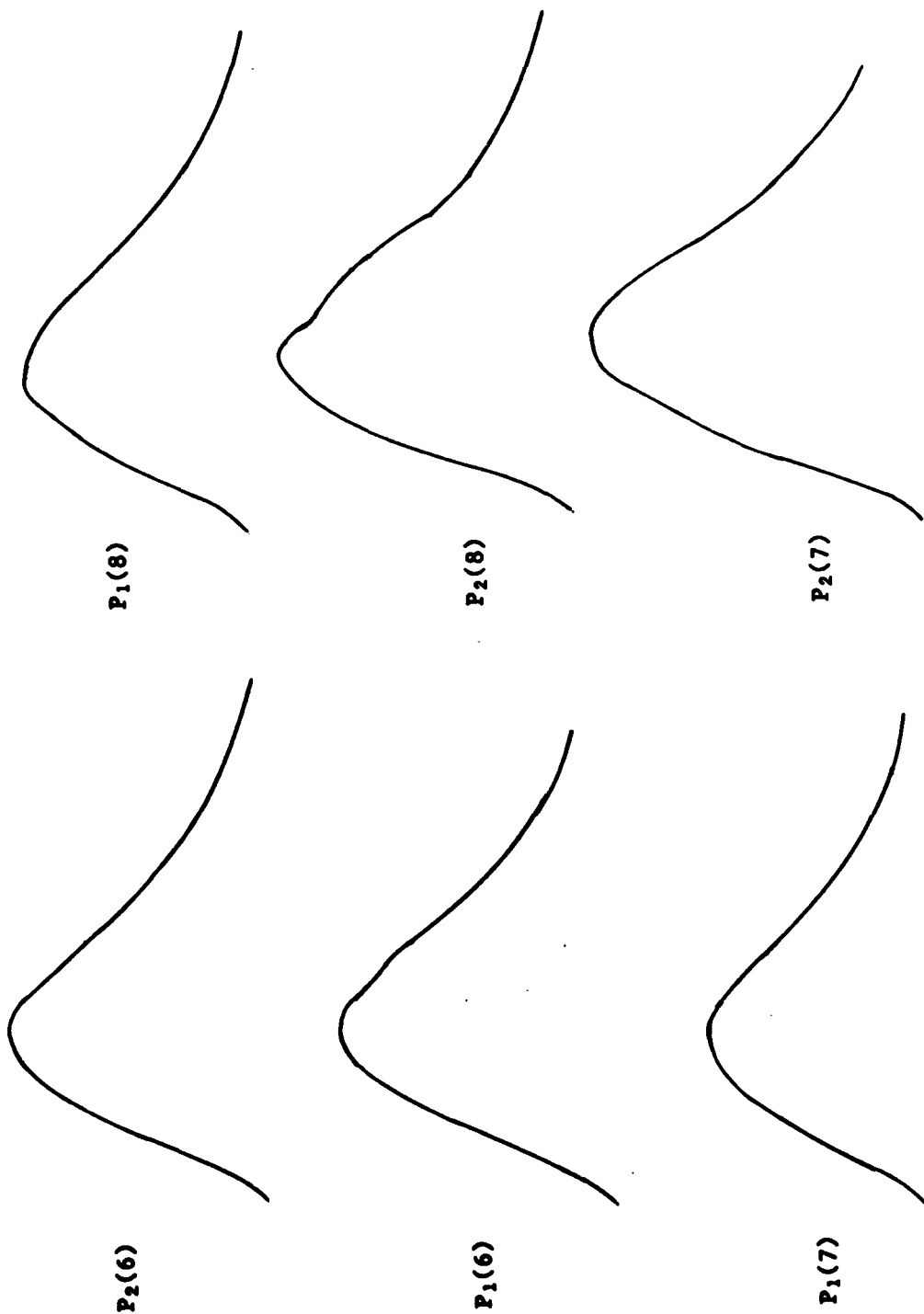


Figure 12

and a table of settings used are contained in Appendix C. An aperture delay range of 2 microseconds and an aperture duration of 50 nsec would be required to yield a pulse shape.

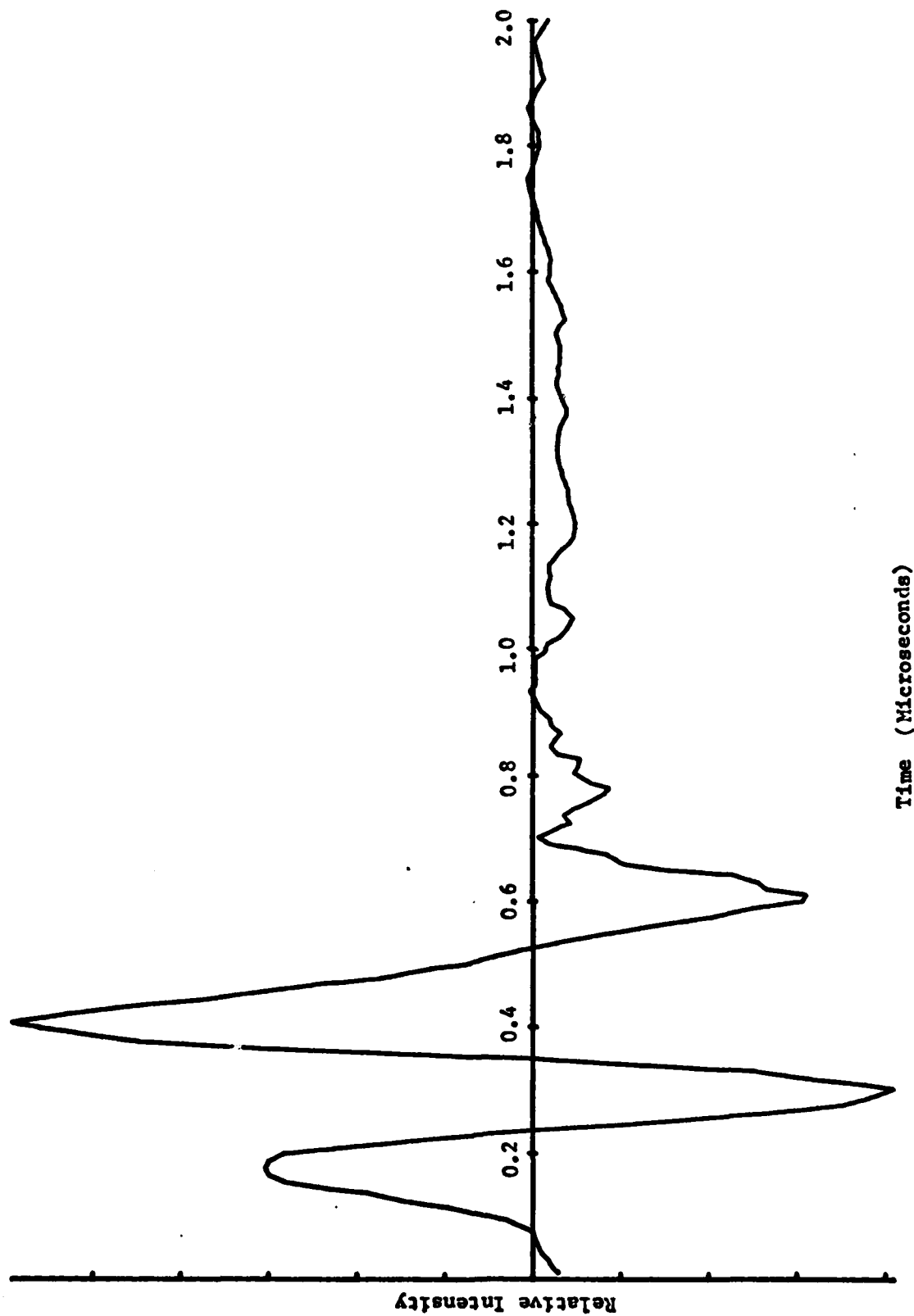
ORTL Experiment

This section is divided into three parts relating to a genesis of the experimental apparatus in order to overcome noise problems. The first part was an attempt to use two separate paths for a reference pulse and the ORTL probe pulse. The second part is a single path experiment sampling discrete points in time of the pulse using separate runs for reference and ORTL probe pulses. The third part uses a single path approach with a chopper on the pump beam to obtain a ratio.

The experiment originally consisted of two separate paths with the advantage of simultaneity. Pulse variations in the pump laser would affect both the probe and reference pulses. These pulses would be expressed as a ratio by $\text{Log}_{10} |A|/|B|$ after noise reduction, where A was the probe pulse from the ORTL cell and B was the reference pulse. Any variations in the pump laser pulse would be cancelled in the ratioing process. The experimental design overcame a weakness in the experimental design used at AFWL [36]. The weakness in Dr. Drummond's method is due to energy variations that can occur on a given line from pulse to pulse, thus subjecting the data to these variations. Dr. Drummond's method employed a single path, using a Lumonics laser for a pump laser. The cell was a five centimeter long teflon tube in which HF gas was flowed at pressures of 10 torr and 30 torr. The signal was averaged over 14 pulses. The cell was then evacuated and a reference signal taken over 14 pulses [6], [36]. Results of the two path procedure showed variations in pulse height observed from the Lumonics laser that are on

the order of 40% to 50% on a given line. The laser also drifts in frequency, a problem that was very severe at small slit widths of the monochromator. Plots of the ratios of the pulse shapes $A/|B|$ (HF/He) varied from trial to trial yielding no repeatable results. This was not unexpected due to the large amount of noise present in the signal. The ratio of HF/He with helium in both cells again showed results that were not repeatable. This last ratio would ideally yield a straight line plot. The InSb detector and the HgCdTe detector and their pre-amplifiers each responded to noise differently thus making a ratio of signals using these two detectors unreliable.

The second part of the experiment was similar in approach to the method used by Dr. Drummond [36]. The InSb detector was used to detect the signal output from the monochromator. The signal was from a single path through the ORTL cell (I) (see figure 8). The signal was averaged over 800 pulses for each stage. The first stage was with helium in the cell at 50mm Hg pressure. The second stage was with an HF/He mixture of $\frac{1}{2}\%$ HF by volume, also at 50mm Hg pressure. The final stage was a repeat of the helium to check for drift due to noise. The results for $P_2(8)$ are shown in figures 13 and 14. The noise in the signal was again sufficient to cause large variations from trial to trial such that the results of a given trial were not repeatable. A second phase to this part was then carried out. The ORTL cell was filled with HF/He mixture at 50mm Hg pressure and the reference cell filled with helium at 50mm Hg pressure. A series of 15 pulses were then averaged through the reference cell, then the ORTL cell, first with pump on and then with the pump blocked. The pulse was sampled at 2/10 microsecond intervals from 0.2 to 1.8 microseconds. The results are listed in Table IV and



Time (Microseconds)

Figure 13 Helium Time Average Over Pulse for $P_2(8)$

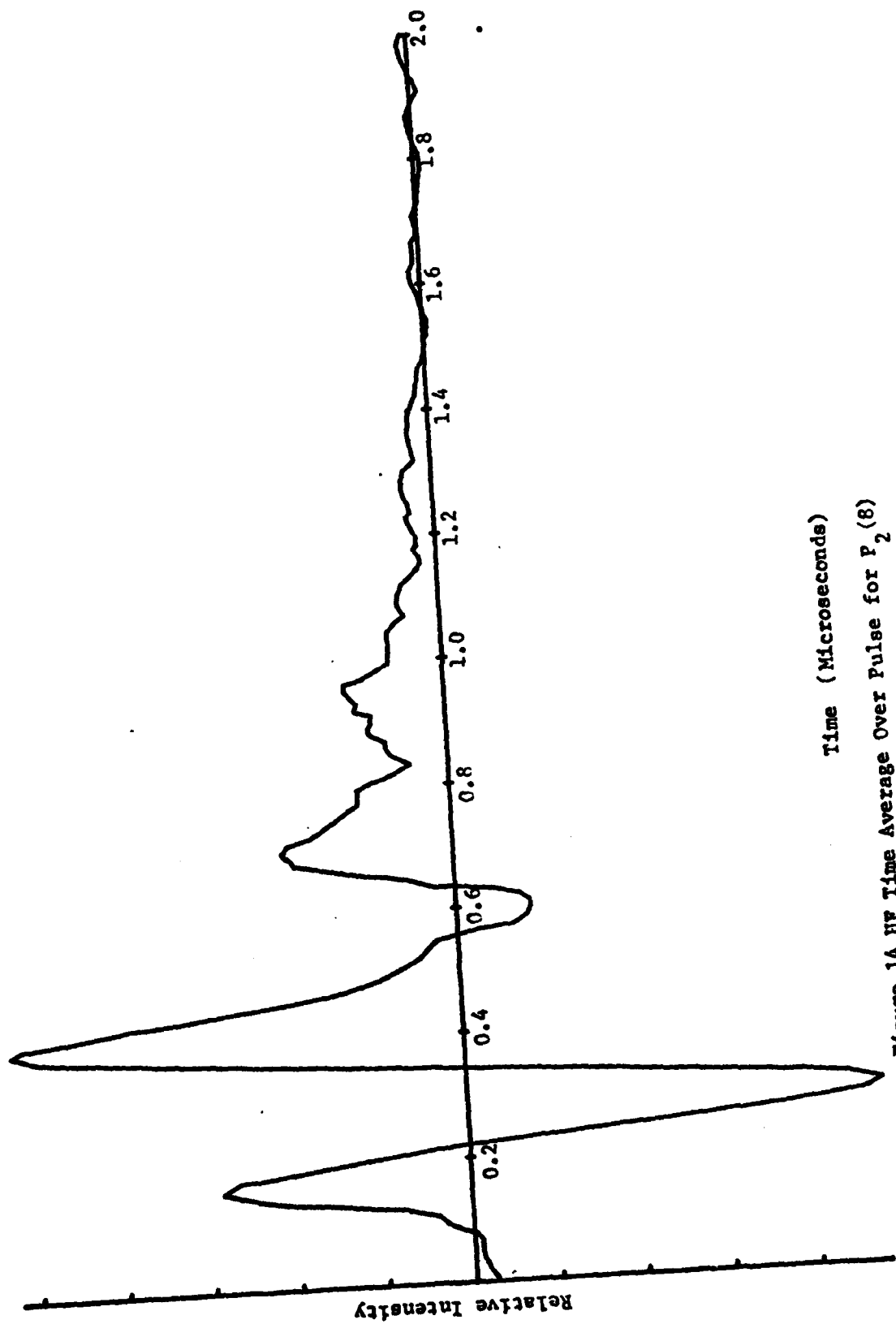


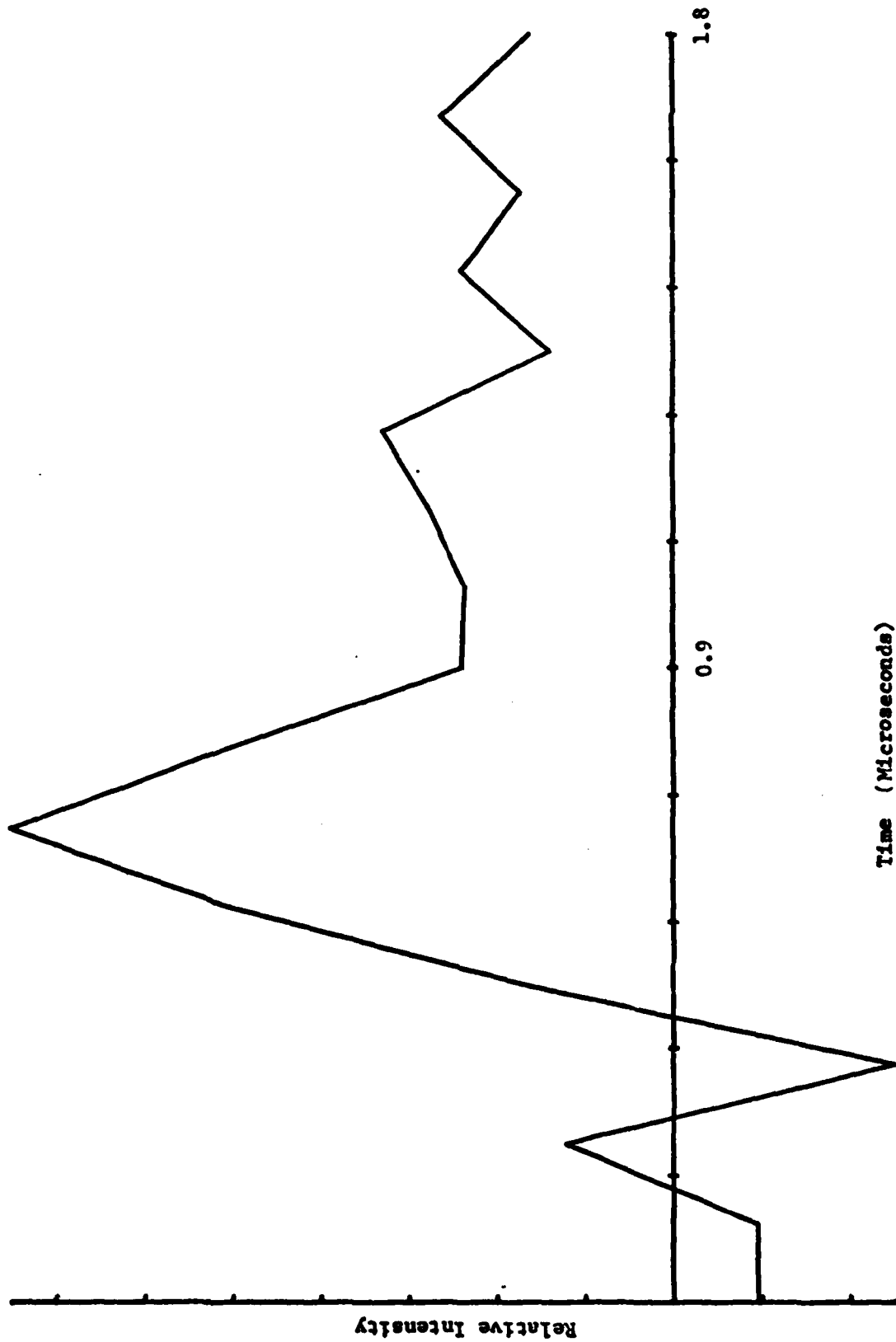
Figure 14 HF Time Average Over Pulse for P_2 (8)

Table IV

time (microseconds)	HF (pump)	HF (no pump)	He
0.2	-0.3	-0.3	-0.3
0.3	-0.3	-0.3	-0.3
0.4	0.6	0.6	0.5
0.5	-0.5	-0.5	-0.9
0.6	0.6	0.5	0.6
0.7	1.5	1.4	1.8
0.8	2.4	2.4	2.7
0.9	2.1	1.7	1.8
1.0	1.4	1.3	0.8
1.1	1.0	0.8	0.8
1.2	1.2	1.2	1.0
1.3	1.1	0.7	1.2
1.4	0.9	0.8	0.5
1.5	1.0	1.0	0.8
1.6	1.1	1.1	0.6
1.7	1.0	0.9	0.9
1.8	0.9	0.8	0.6

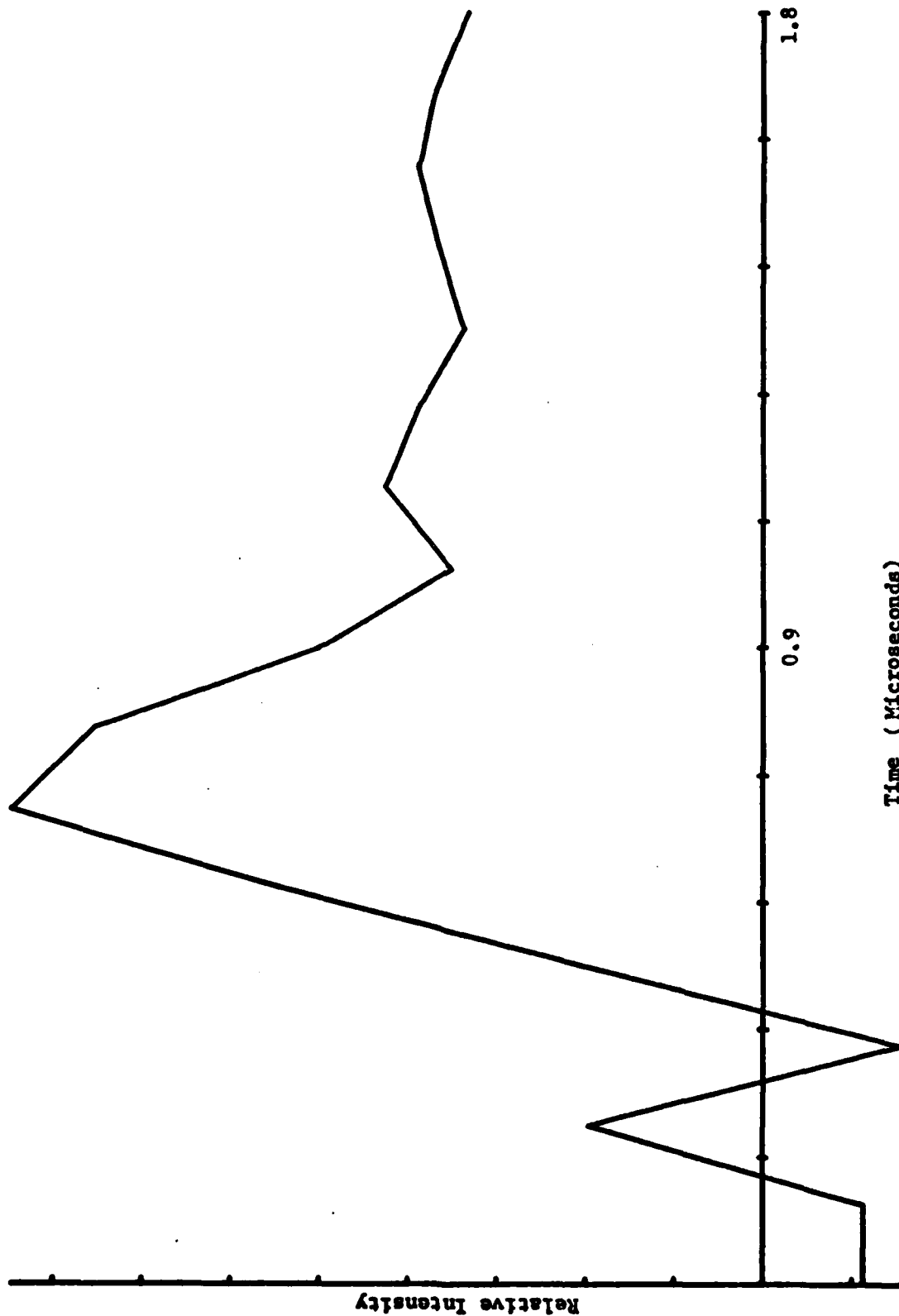
graphed in figures 15, 16, and 17 for the $P_2(8)$ line. Figure 15 is the pulse shape through helium gas. Figure 16 is the pulse shape through HF with the pump beam on. A conclusion will be drawn on the deconvolution of these curves later in this section.

The third part of the experiment evolved from the procedure described above. A chopper was placed in the path of the pump beam so as to block alternate pulses. The signal would then enter either channels A or B of the boxcar averager as selected by TTL logic from the chopper. Channel A received the pumped signal and channel B received the unpumped signal. A pulse shape was then plotted for $P_2(8)$. The procedure was repeated with the pump pulse blocked on every pulse and then a third trial with helium gas in the ORTL cell. All pressures



Time (Microseconds)

Figure 15 Discrete Time Average: Helium for P₂(8)



Time (Microseconds)

Figure 16 Discrete Time Average: $^{19}\text{F}/^{16}\text{O}$ for $P_2(8)$ Pump On

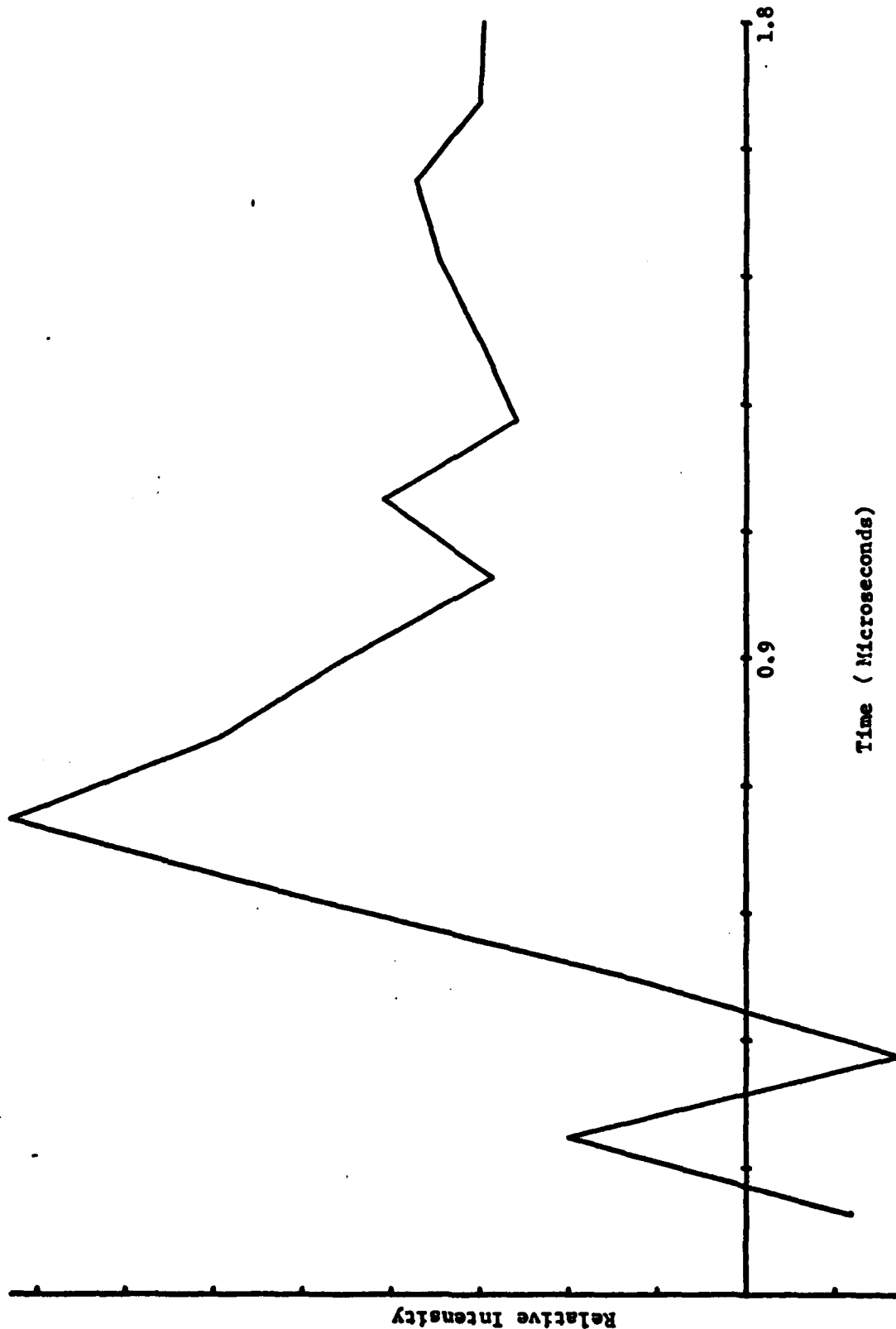
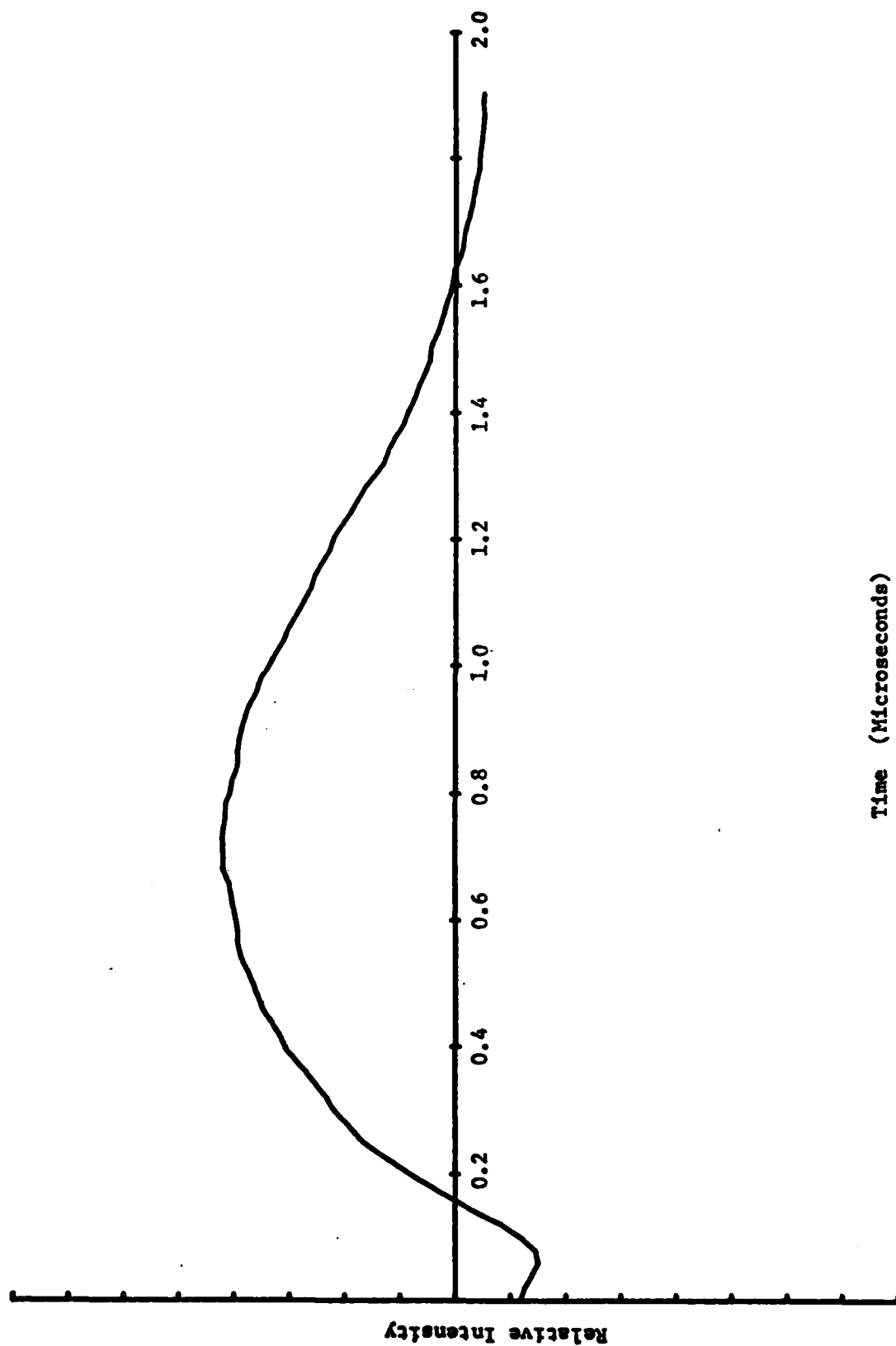


Figure 17 Discrete Time Average: HF/Helium for P₂ (8) Pump Off

were at 50mm Hg. The curve in figure 19 contains information about the absorption of the pump beam in the ORTL cell. This information is convolved with information about the interaction of the pump beam with the helium in the cell and the interaction of the probe beam with the HF/He mixture. The absorption information can be obtained by deconvolving the three sets of data. The method of deconvolution is as follows:

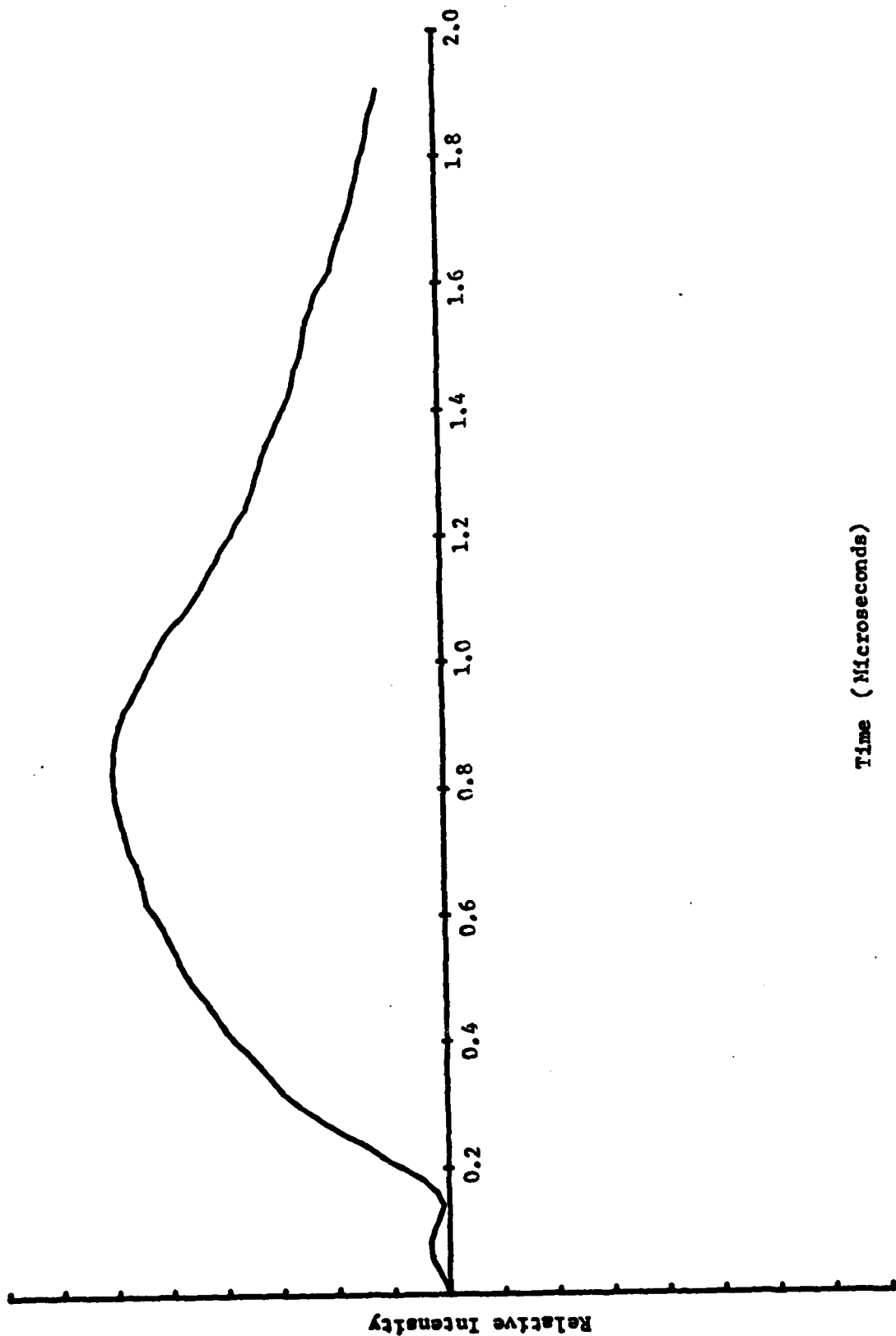
$$F^* = \frac{F(\text{HF/He})_{\text{pump+probe A}}}{F(\text{HF/He})_{\text{probe B}}} - \frac{F(\text{HF/He})_{\text{probe A}}}{F(\text{HF/He})_{\text{probe B}}} - \frac{F(\text{He})_{\text{probe A}}}{F(\text{He})_{\text{probe B}}}$$

where F^* represents a point by point subtraction of figures 18 and 20 from figure 19 over 200 data points. This procedure results in a numerical deconvolution of the curves, F^* . F^* is a curve representing absorption of the pump beam by HF plotted vs time. The region of the curve above the abscissa represents reduced absorption and the region of the curve below the abscissa represents increased absorption. The result is a plot of decreased absorption/increased absorption over time. Where the curve goes above zero is an area of decreased absorption and there exists the possibility of a partial population inversion and thus gain in this region. The results are shown in figure 21 compared to figure 22 which the $P_2(8)$ line reduced by Dr. Drummond. His results show a gain of 1% to 2% on $P_2(8)$ and $P_2(7)$. These results were obtained by subtracting $\log |A|$ from $\log |B|$ where A is the HF ORTL pulse shape and B is the reference pulse shape. The nomenclature used in F^* is used to show that the data is expressed as a ratio. The curve in figure 21 resembles the curve in figure 22. This result suggests the possibility of gain similar to that obtained by Dr. Drummond on $P_2(8)$.



Time (Microseconds)

Figure 18 Helium Time Average Over Pulse $P_2(8)$ Ratio



Time (Microseconds)

Figure 19 HF/HeIum Time Average Over Pulse P_2 (8) Ratio Pump On

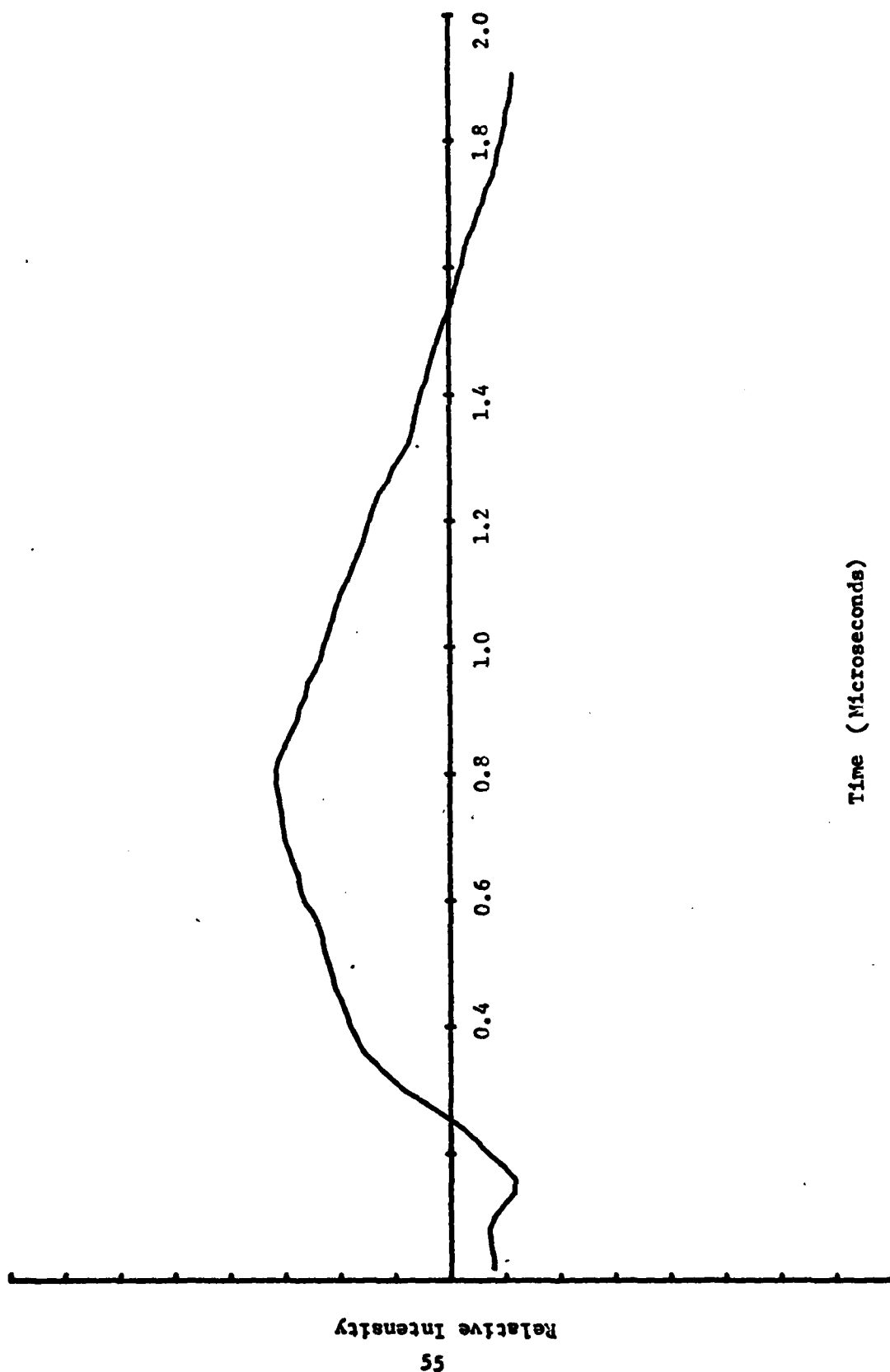


Figure 20 HF/Helium Time Average Over Pulse P_2 (8) Ratio Pump Off

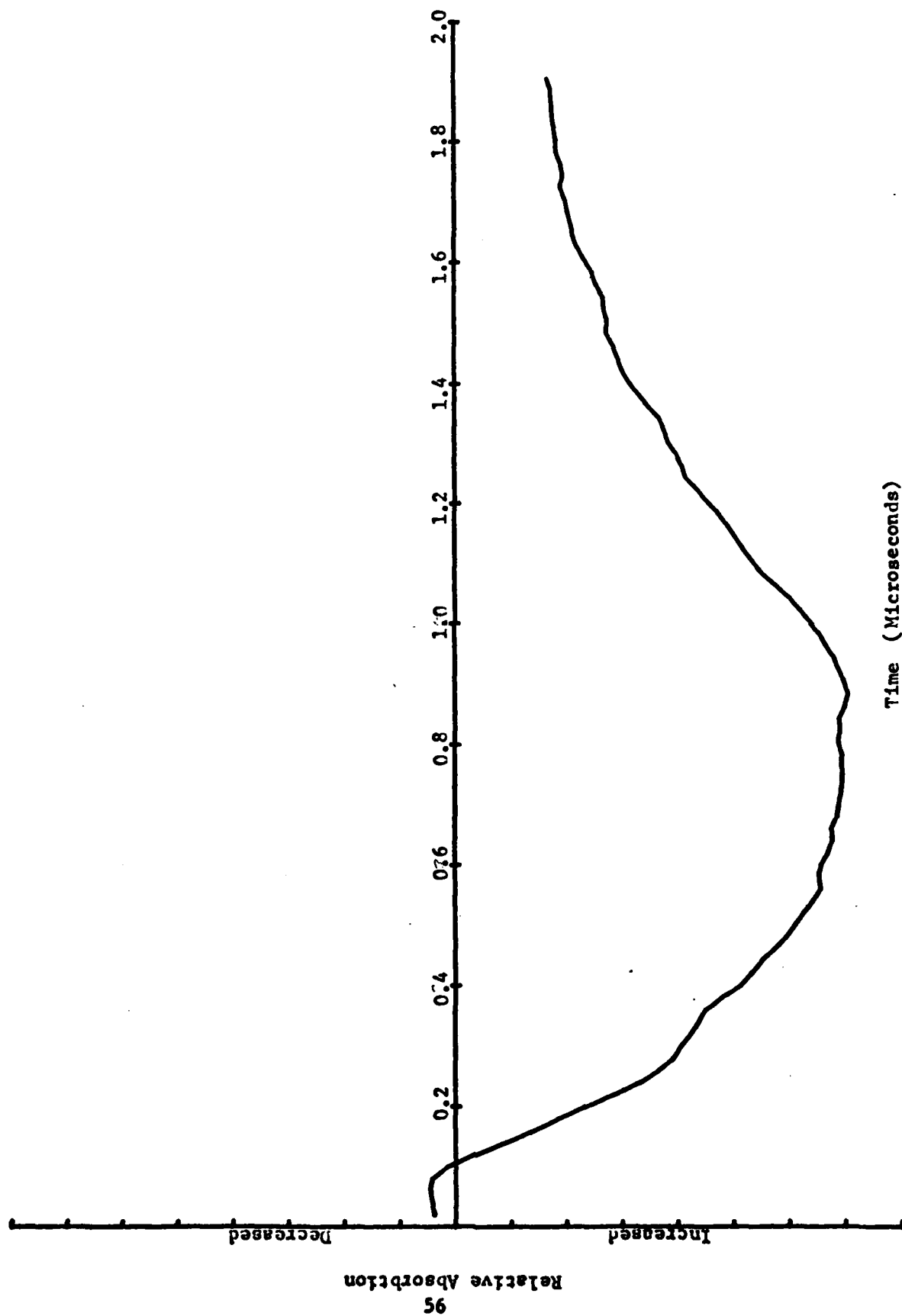


Figure 21 Decreased-Increased Absorption vs Time for P₂(8)

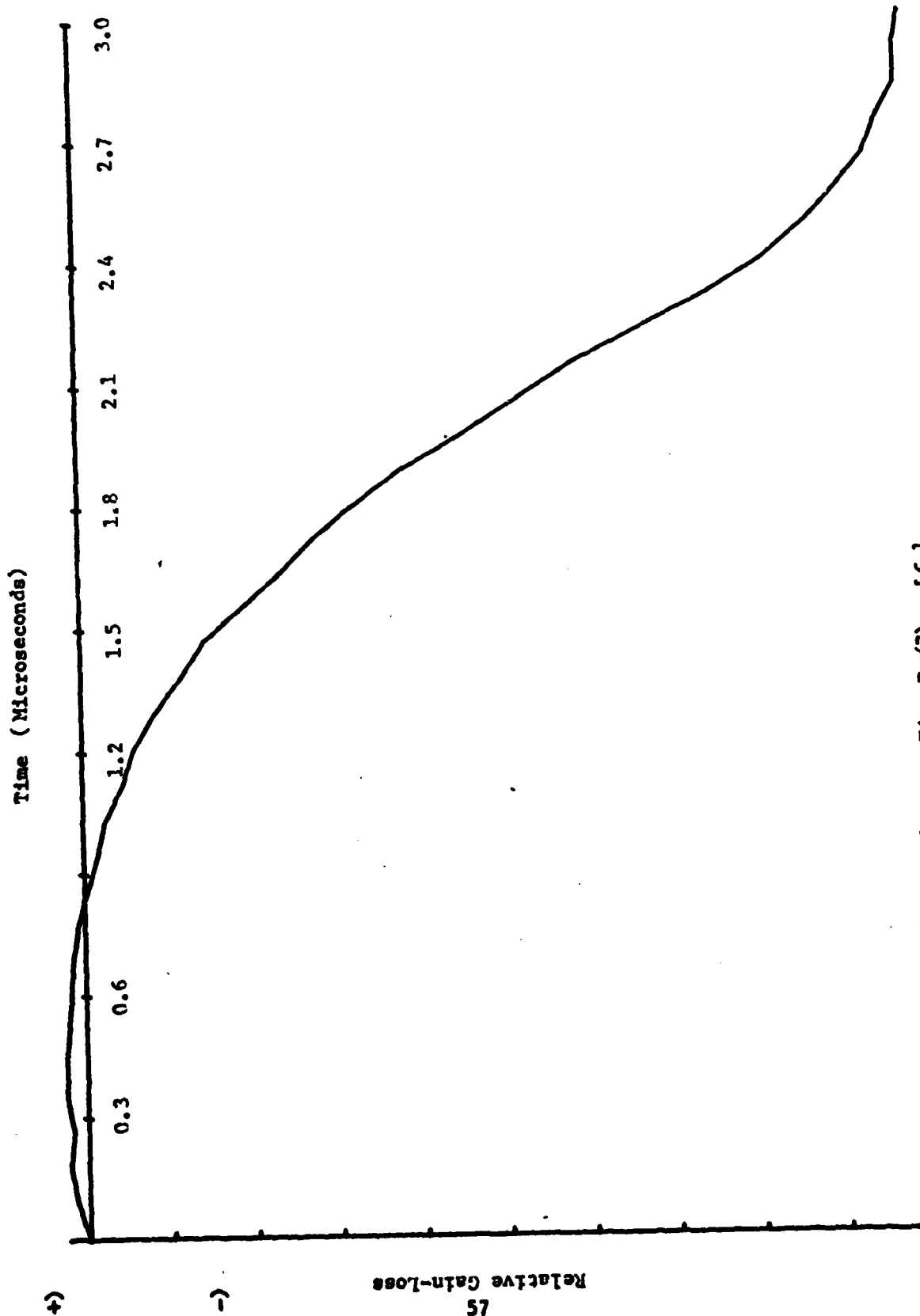


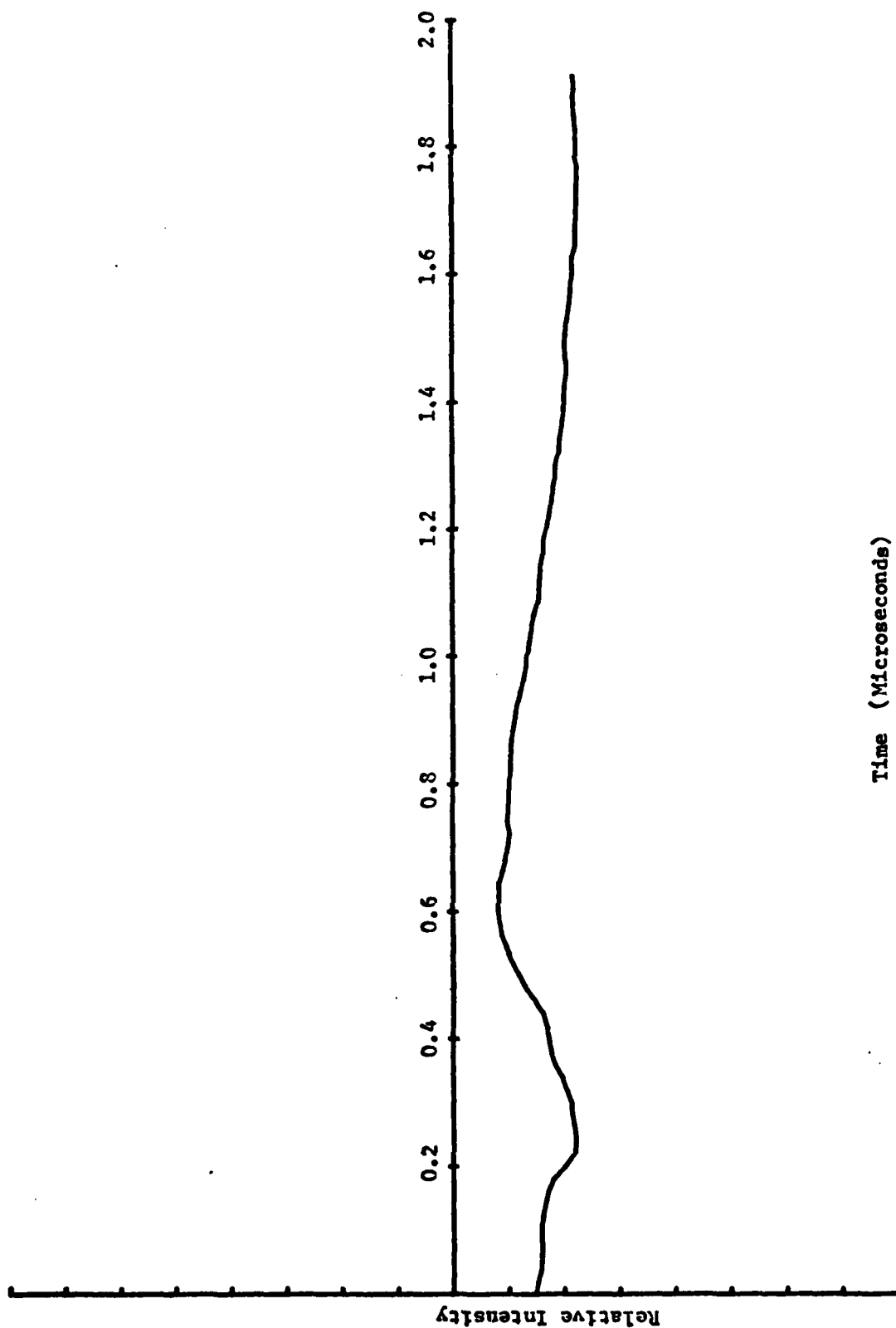
Figure 22 Gain-Loss vs Time $P_2(7)$ [6]

The pulse to pulse variations far exceed the few percent gains observed in figure 21, however, the data was collected over 800 pulses and expressed as a ratio of alternate pulses. This method reduces, though not eliminates, the sensitivity of the data to pulse to pulse variations. The $P_2(7)$ line is shown in figures 23-25 reduced to the curve shown in figure 26. The signal level on the $P_2(7)$ line was too low to obtain reliable results and the resultant deconvolution (figure 26) must be considered inconclusive. The final portion of this part of the experiment investigated the possibility that the pump beam acted as a probe due to inaccuracies in the ZnSe plate angle used to remove the pump beam. The chopper was placed in the probe beam path and the TTL logic sequence reversed. The resultant curve is shown in figure 28. Figure 29 shows the results of the above treatment applied to the data in Table IV.

The conclusion drawn from the curve in figure 28 is that the ZnSe plates in the optical train could not be placed at precisely Brewster's angle and thus some leakages of the pump beam into the probe beam path occurred. The result is that a portion of the pump beam was received at the detector and the pump was then acting as its own probe.

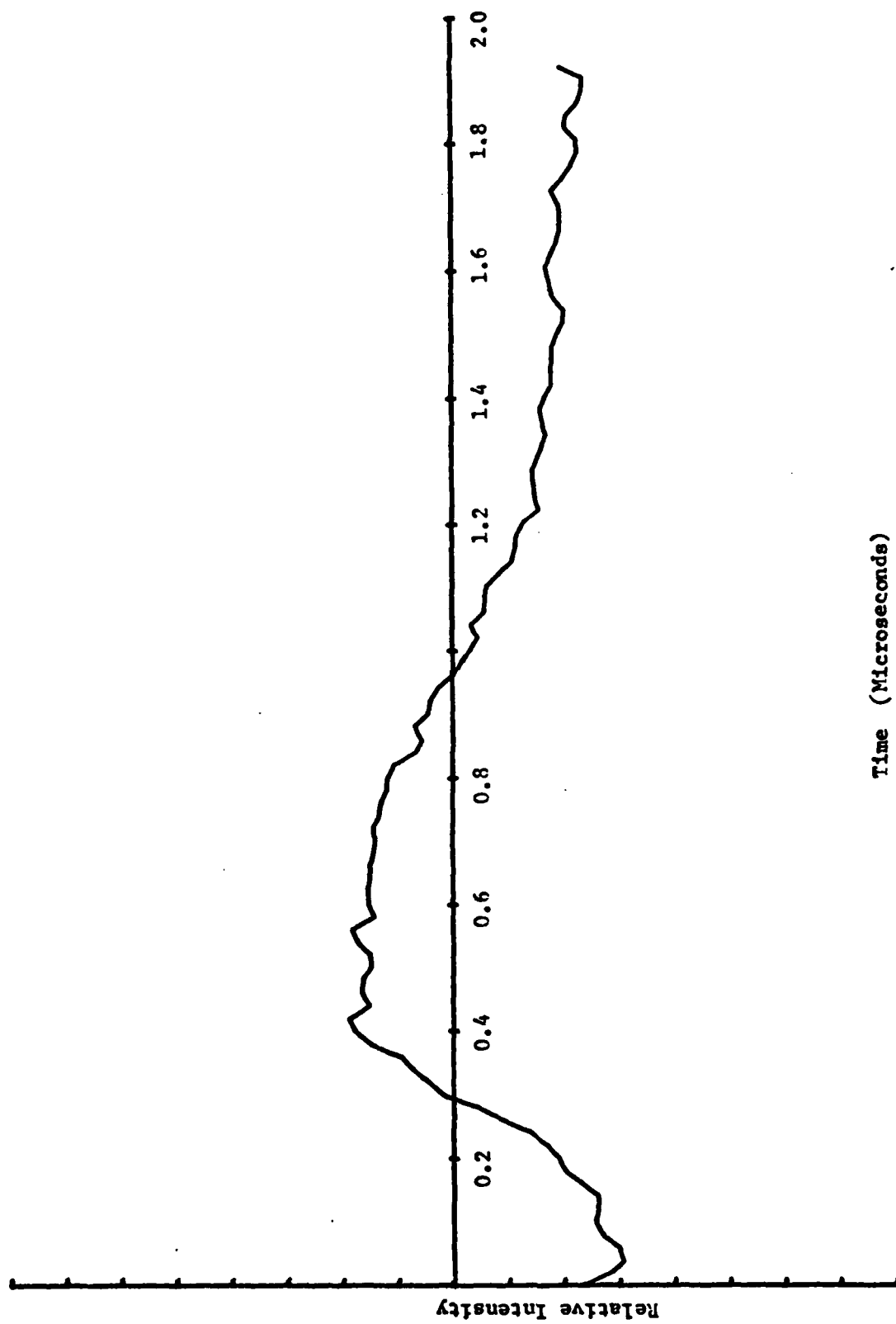
Kinetics Modeling

Depopulation of a three level system is modeled by the two level system of rate equations described in Chapter II. The model assumes an initial level of N , the population of the upper level. This initial population is N_1^0 . The N_2 population is established by the pump laser pumping primarily on $P_1(J)$ and $P_2(J)$ lines. The assumption used is that N_1^0 is reached instantly and begins to decay over two microseconds. The model serves to demonstrate the depopulation rates with times long



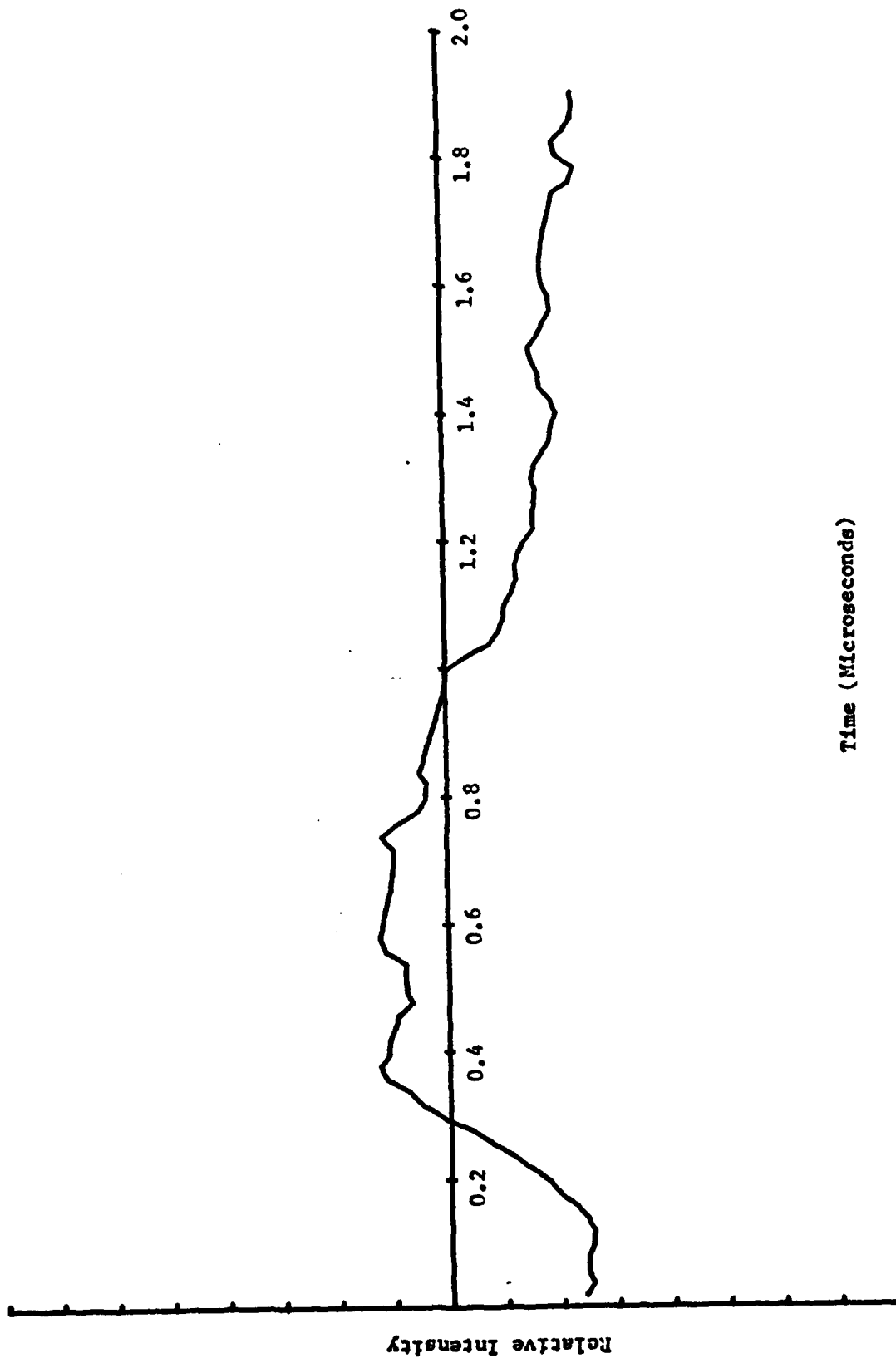
Time (Microseconds)

Figure 23 Helium Time Average Over Pulse P_2 (7) Ratio



Time (Microseconds)

Figure 24 HF/Helium Time Average Over Pulse P_2 (7) Ratio Pump On



Time (Microseconds)

Figure 25 HF/Helium Time Average Over Pulse $P_2(7)$ Ratio Pump Off

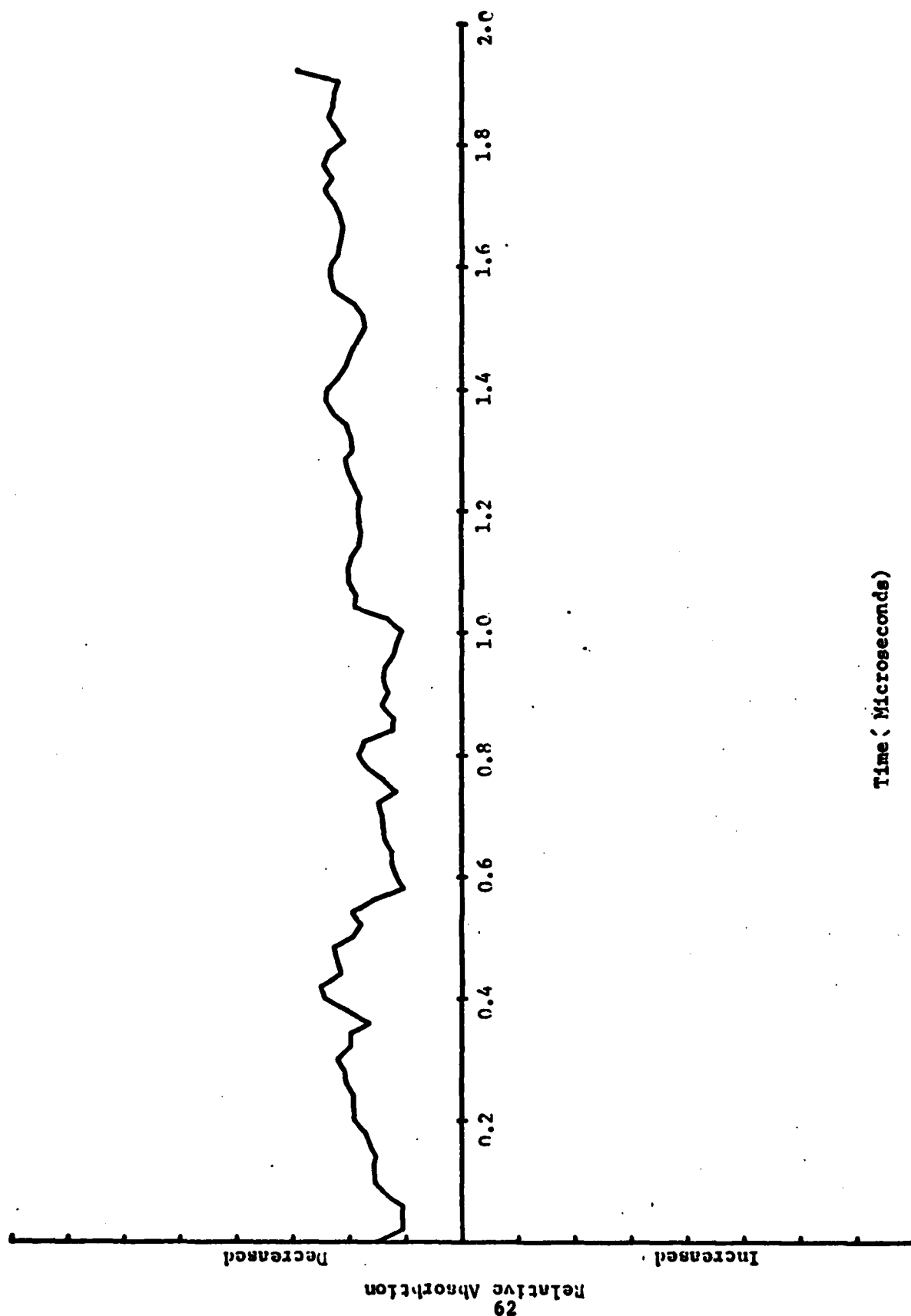


Figure 26 Decreased-Increased Absorption vs Time for $P_2(7)$

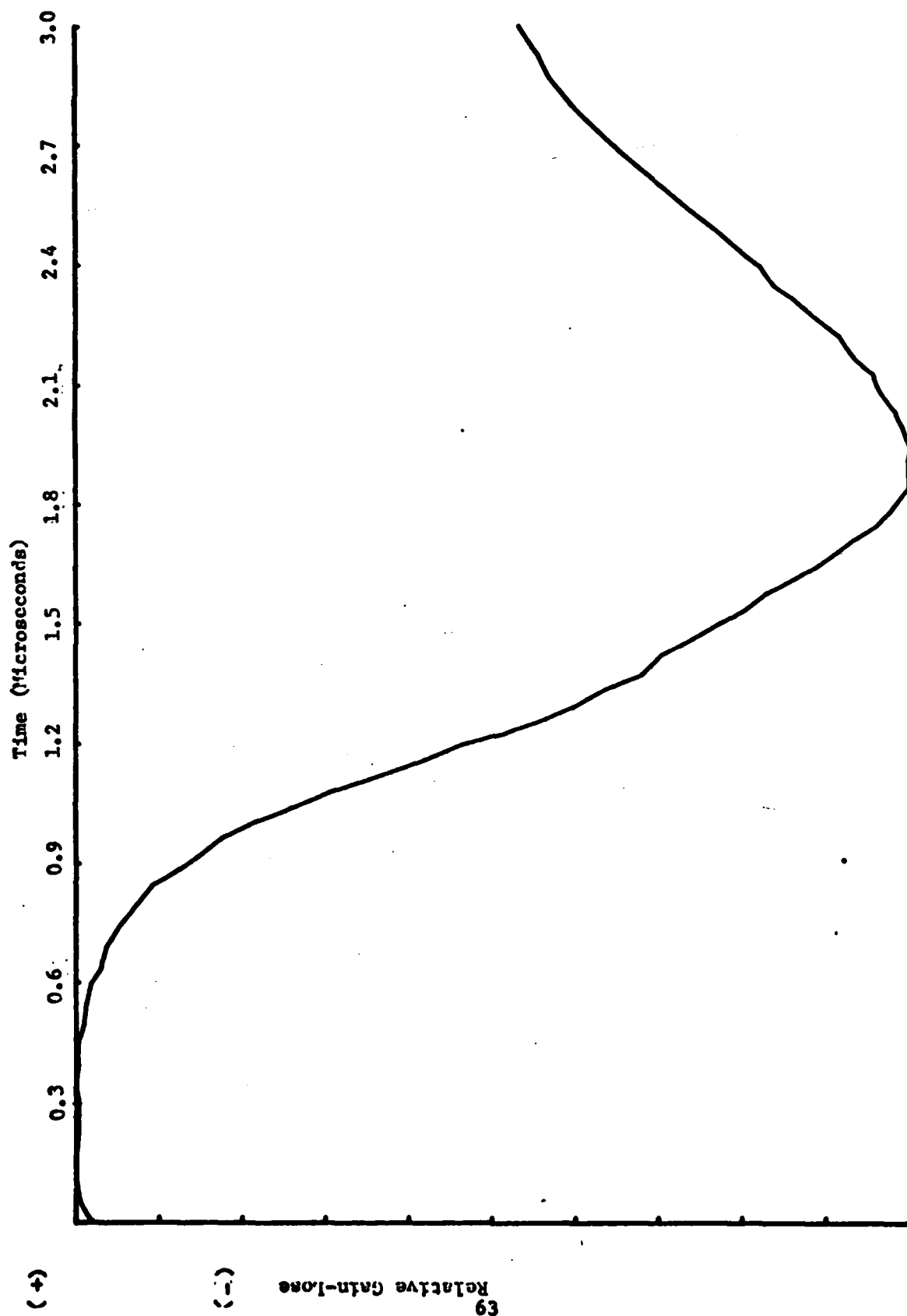
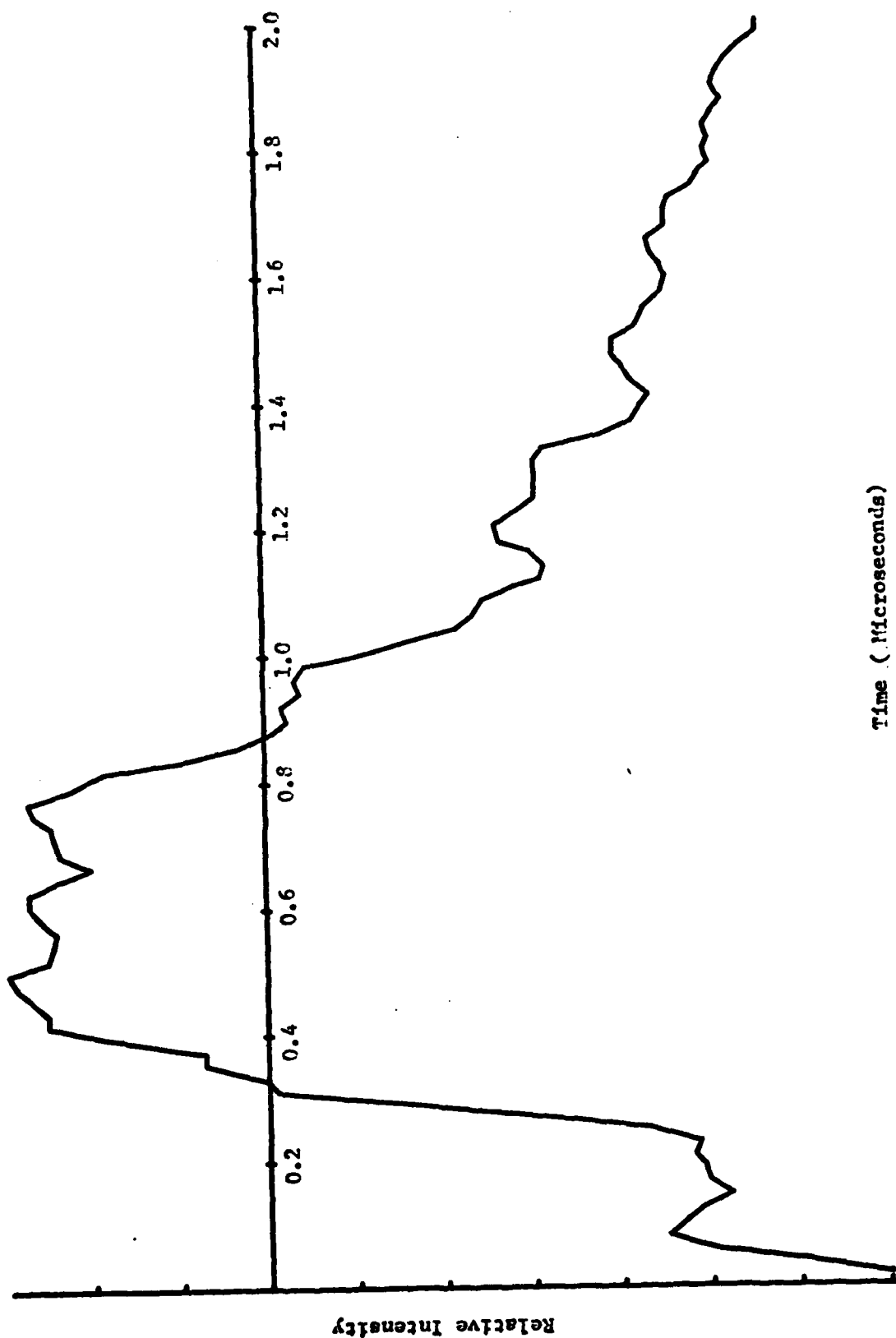


Figure 27 Gain-loss vs Time

for $F_2(7)$ [6]



Time (Microseconds)

Figure 28 Pump Beam Leakage in to Probe Path $P_2(P)$

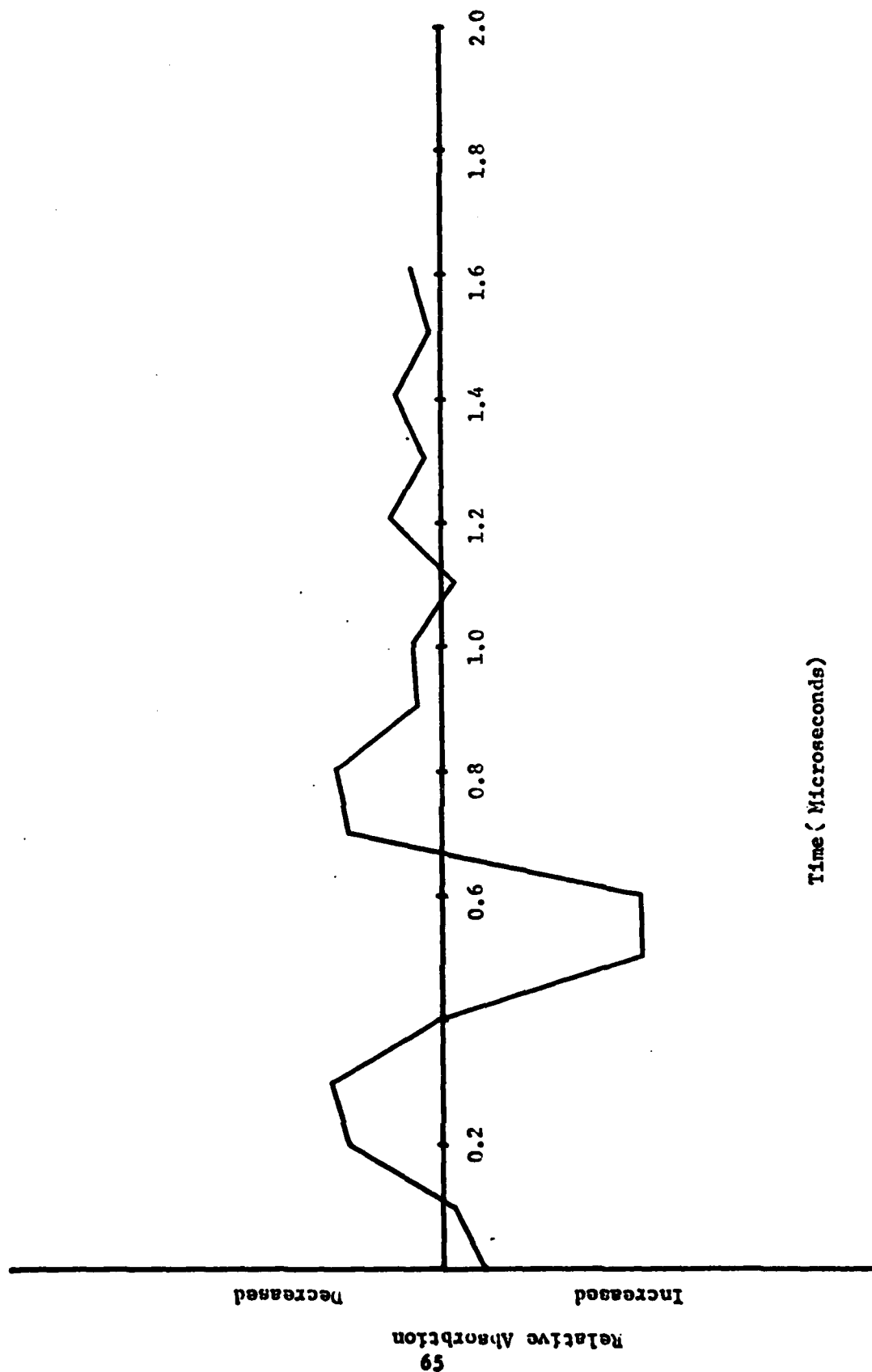


Figure 29 Decreased-Increased Absorption vs Time

$r_2(8)$ From Table IV Data

compared to rotational relaxation. This further assumes a near Boltzman distribution among rotational populations. This assumption is justified by comparing rates for V-V and R-R used by Lindquist, et al., 24:36,43 , where

$$\begin{aligned}k_{VV} &= 2.8028 \times 10^{-13} \text{ cm}^3/\text{molecule-second} \\k_{RR} &= 2.6543 \times 10^{-10} \text{ cm}^3/\text{molecule-second} \\ \text{and } n &= 8.1953 \times 10^{15} \text{ molecules (HF)/cm}^3 \\ t &= 2 \times 10^{-6} \text{ seconds}\end{aligned}$$

$$\text{then } \frac{\exp(-k_{VV}nt)}{\exp(-k_{RR}nt)} \approx 68$$

or almost two orders of magnitude difference in relaxation rate.

The rate equations use rate constants obtained from Kerber and Whittier 26:11 which are in $\text{cm}^3/\text{molecule-seconds}$. These constants are converted to $\text{cm}^3/\text{molecule-seconds}$ for use in these equations. Rate constants throughout the literature are varied, showing a great extent of disagreement on the correct values 22:86 , 34:151 , 27:471 , 31:255 , 30:4457 , 26:11 , 24:36 .

The results of the analysis are shown in table V and plotted in figures 30 and 31.

A comparison with figure 17 shows that the computer model of the rate equations discussed above shows excellent agreement with experimental results for the $P_2(8)$ line yielding a pulse shape that has a peak at 800 nano seconds. The rate equations are

$$\begin{aligned}N_1 &= N_1^0 \exp(-\delta t) \\ N_2 &= \frac{(N_1^0)^2 \exp(-2\delta t)}{N_0(1+\sigma^2/\epsilon)} \{1 - \exp -(\Gamma - 2\delta)t\}\end{aligned}$$

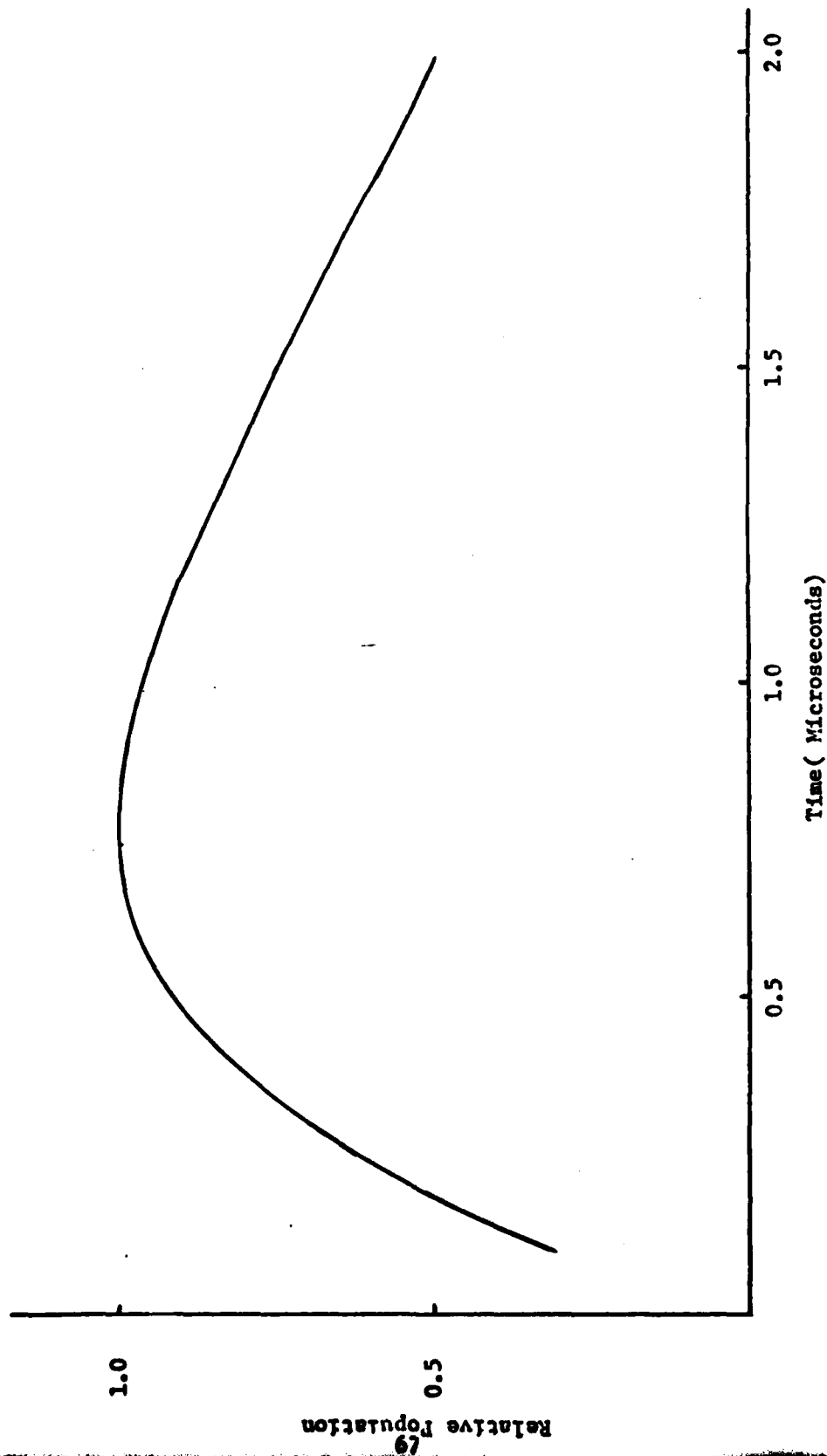


Figure 30 Rate Equation Plot: N_2

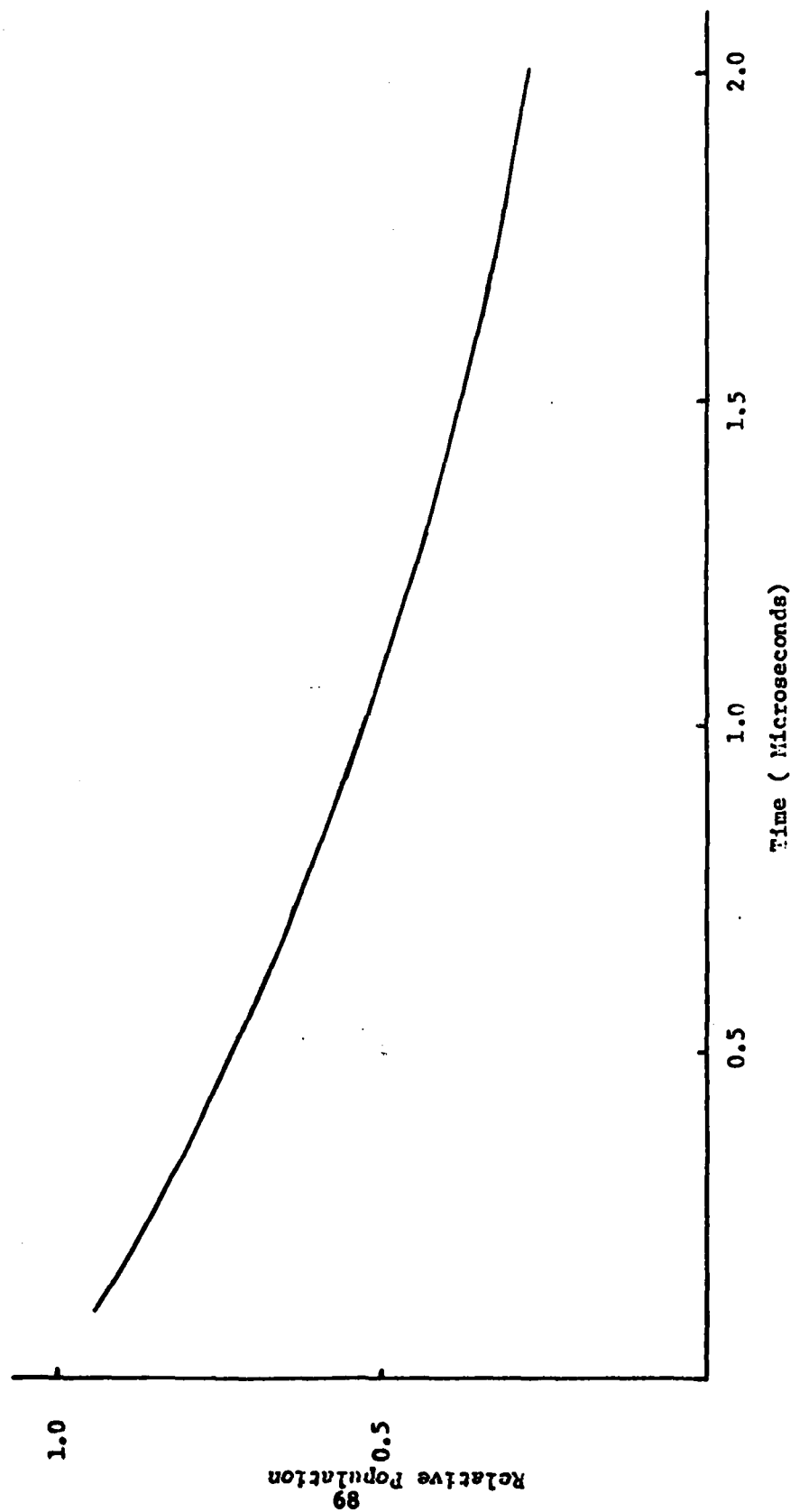


Figure 31 Rate Equation Plot: N_1

Table V

time (microseconds)	N ₂ (Relative percent)	N ₁ (Relative percent)
1	0.31022	0.93762
2	0.54489	0.87912
3	0.71780	0.82428
4	0.84052	0.77286
5	0.92271	0.72465
6	0.97242	0.67944
7	0.99633	0.63705
8	1.00001	0.59731
9	0.98801	0.56005
10	0.96411	0.52511
11	0.93138	0.49235
12	0.89232	0.46164
13	0.84897	0.43284
14	0.80294	0.40584
15	0.75554	0.38052
16	0.70777	0.35678
17	0.66043	0.33452
18	0.61413	0.31566
19	0.56931	0.29409
20	0.52630	0.27574

where Γ represents the rate constant for level two combining V-V, V-T, diffusion, and HF-H₂O V-V exchange. The rate constant for HF-HF V-V and V-T was calculated as follows (T = 931.8K, see Appendix E)

(V-V)

$$\text{HF}(0) + \text{HF}(2) = 2\text{HF}(1)$$

$$\begin{aligned} k(1)_{\text{HF-HF}} &= 1.5 \times 10^{12} T^{\frac{1}{2}} \\ &= 4.5788333 \times 10^{13} \text{ cm}^3/\text{mole-degree} \end{aligned}$$

$$\text{HF}(1) + \text{HF}(2) = \text{HF}(0) + \text{HF}(3)$$

$$k(2)_{\text{HF-HF}} = 0.25 k(1) = 1.1447 \times 10^{13} \text{ cm}^3/\text{mole-degree}$$

(V-T)

$$\text{HF}(2) + \text{HF} = \text{HF}(1) + \text{HF}$$

$$\begin{aligned} k_{\text{V-T}} &= 2(10^{14} T^{-0.8} + 10^{0.4} T^{3.5}) \\ &= 9.6657 \times 10^{11} \text{ cm}^3/\text{mole-degree} \end{aligned}$$

diffusion effects may be neglected as they are small compared even to V-T rates [27:471].

The rate constant for HF-H₂O was calculated as follows:

6HF + Al₂O₃ → 3H₂O + 2AlF₃ as the aluminum passivates the HF in the gas [16:476].

The density of Al₂O₃ is 3.7g/cm³. The inner surface area of the cell is 15.97 cm² and a volume may be obtained by $(\sqrt{A})^3$ to obtain 63.82 cm³ or 236.134 grams of Al₂O₃. The g.m.w. of Al₂O₃ is 102 grams then the number of molecules present is $2.315 \times N_A$ or 1.39435×10^{24} molecules in this constructed volume. A cube of this volume is 3.996 cm on a side and contains a line of 1.117×10^8 molecules. This may be used to obtain a volume comprised of the inner surface area of the cell and one molecule thick. This volume contains 1.16945×10^{16} molecules of Al₂O₃. There are however only 2.9198×10^{16} molecules of HF as calculated in Chapter III

and as 6HF are required for each Al_2O_3 , the number of water molecules is then $3(N_{\text{HF}}/6) = 1.4598 \times 10^{16}$ molecules of water. Over the cell volume this yields 4.098×10^{15} molecules/cm³. The rate constant for HF-H₂O is

$$k' = 10^{-28} \exp(0.57 \times 10^{-3} T) / 3.104 \times 10^{11} \text{ cm}^3/\text{molecule-second}$$

[43:3279]

$$= 2.2815 \times 10^{-12} \text{ cm}^3/\text{molecule-second}$$

At 1500K, the probability of an HF-H₂O collision is 116.7 times greater than for an HF-HF collision [43:3279] and 43.85 times greater at 294K [42:4516]. By interpolation, the probability at 931.8K is 82.36 or

$$k_{\text{HF-H}_2\text{O}} = 82.36 k' = 1.879 \times 10^{-10} \text{ cm}^3/\text{molecule-second}$$

$$k_{\text{HF-H}_2\text{O}} N_{\text{H}_2\text{O}} = 769977.08$$

Returning to the HF-HF rate constants, the units are converted following summing:

$$k_{\text{HF-HF}} = k(1) + k(2) + k(V-T) / 6.023 \times 10^{23} = 9.663288 \times 10^{-11} \text{ cm}^3/\text{molecule-second}$$

$$k_{\text{HF-HF}} N_{\text{HF}} = 791939.4$$

$$\text{and } \Gamma = 791939.4 + 769977.08$$

δ is obtained by $\text{tm}\Gamma = \ln(2\delta/\Gamma)$

where tm is the time to the peak of the pulse, here tm is 800 nsec.

Conclusions and Recommendations

A study of the Pulsed HF ORTL has been completed. The background theory for the performance of the system has been presented and applied. Optical pumping of the ORTL cell by the HF $P_2(8)$ and $P_2(7)$ transitions has been studied through absorption experiments in three configurations. The two path experiment yielded results on $P_2(7)$ and $P_2(8)$ that were not repeatable. It was suggested that electromagnetic radiation from the pump laser may have been the responsible agent adversely affecting the signal to noise ratio in this experiment. The second experiment followed Dr. Drummond's work at AFWL, pumping the ORTL cell alone, first with helium in the cell for reference then with the HF/helium mixture and then followed by a third set of data with helium to check for drift in the system. The results were not repeatable for either $P_2(7)$ or $P_2(8)$ due to a poor signal to noise ratio. The third experiment used alternate pulses through the ORTL cell in a ratio of pump on over pump off for helium and HF/helium. The results for the $P(8)$ line show good agreement with Dr. Drummond's data for the $P_2(8)$ line. The $P_2(7)$ line lacked enough intensity to produce reliable results in the existing noise environment. The results for the $P_2(8)$ line indicate the possibility of a partial population inversion with gain of a few percent. Agreement of the data for the $P_2(8)$ line pumping HF with the kinetics model presented in Chapter II was satisfactory.

The Lumonics laser used as a pump laser provided a pulse that was too weak on lines other than $P_2(8)$ and $P_1(8)$ to investigate ORTL effects. Dr. Drummond's investigation indicated no gain on the $P_1(8)$ line thus no attempt was made to probe the ORTL cell on this line.

Several recommendations are made based on these results and conclusions.

The noise created by the electromagnetic pulses from the pump laser should be reduced to obtain a better signal to noise ratio. One method by which this may be accomplished is to use a Faraday cage. The cage should house all sensitive electronic equipment used in actual data acquisition and reduction. This should include at a minimum, the detectors, their preamplifiers and the boxcar averager.

The signal averaging method may be improved upon by using a two channel transient digitizer. This would allow faster data acquisition and reduction.

The power supply for sensitive electronics should be regulated to protect against transients. Voltage reductions were observed accompanying the start of the air handling system in the building. This could have an adverse affect on data acquisition.

The ventilation in the pump laser room should be improved. Noticeable levels of ozone were present in the room during operation of the laser, reducing working time in that room.

Conclusion

An optically pumped HF ORTL was studied by absorption measurements. The results were compared to a previous investigation. The kinetics of the HF ORTL cell was analyzed showing good agreement with theory.

Bibliography

1. Jones, C. R., "Optically Pumped Mid-IR Lasers," Laser Focus, 68-69, August 1978.
2. Baily, P., Finzi, J., Holleman, G., Hui, K., and Wang, J., "High Energy Optical Resonance Transfer Laser Study," FR-79-73-538, January 1979, Defense Advanced Research Projects Agency, Arlington, Va., 1-3.
3. Baily, P., Finzi, J., Lovejoy, C., and Wang, J., "High Energy Optical Resonance Transfer Laser Study, Volume I, Laboratory Experiments," FR-79-73-999, August 1979, Defense Advanced Research Projects Agency, Arlington, Va., 1-3.
4. Finzi, J., Wang, J. H. S., Hui, K. K., Baily, P. K., Holleman, G. W., and Mastrup, F. N., "CW HF/HCN and HF/DF Optical Resonance Transfer Lasers," IEEE Journal of Quantum Electronics, QE-16, 912-913, September 1980.
5. Wang, J. H. S., Finzi, J., Baily, P. K., Holleman, G. W., Hui, K. K., and Mastrup, F. N., "CW Optically Resonance-Pumped HF Laser," Applied Physics Letters, 36, 24, January 1980.
6. Discussion with Dr. David Drummond, Air Force Weapons Laboratory, AFWL/ARAC, KAFB, NM, 87117 (14 June 1982).
7. Kasper, J. V. V. and Pimentel, G. C. "HCl Chemical Laser," Physics Review Letters, 14, 352-354, (1965).
8. Kompa, K. L. and Pimentel, G. C., "Hydrofluoric Acid Chemical Laser," Journal of Chemical Physics, 47, 857-858, (1967).
9. Roberts, Thomas G., "Notes on Chemical Lasers Part I - Background," RR-TR-70-18, 30 June 1970, Physical Sciences Laboratory Research and Engineering Directorate, U. S. Army Missile Command, Redstone Arsenal, Al., 15-60.
10. Dorko, E. A., Professor, Air Force Institute of Technology, Class notes from Ph 6.61, Fall Quarter, 1981.
11. Merzbacher, Eugene, Quantum Mechanics, New York: John Wiley and Sons, Inc., 1970, 133.
12. Pedrotti, L. S., Professor, Air Force Institute of Technology, Class notes from Ph 7.43, Winter Quarter, 1982.

13. Lucht, Roy A. and Cool, Terril A., "Temperature Dependence of Vibrational Relaxation in the HF, DF, HF-CO₂, and DF-CO₂ Systems," Journal of Chemical Physics, 60, (3), 1026-1035, February, 1974.
14. Hecht, Eugene and Zajac, Alfred, Optics, Reading, Massachusetts: Addison-Wesley Publishing Company, 1979, 75, 79-80, 397-399.
15. Ahl, Jeffrey L. and Cool, Terril A., "Vibrational Relaxation in the HF-HCl, HF-HBr, HF-HI, and HF-DF Systems," Journal of Chemical Physics, 58, (12), 5540-5548, June, 1973.
16. Weston, G. F., "Materials for Ultrahigh Vacuum," Vacuum, 25, (11/12), 476.
17. Baily, P., Finzi, J., Lovejoy, C., and Wang, J., High Energy Optical Resonance Transfer Laser Study, Volume I, Laboratory Experiments, DARPA ADA074126. Arlington, Virginia: Defense Advanced Research Projects Agency, 1979.
18. Marion, Jerry B. and Heald, Mark A., Classical Electromagnetic Radiation, New York: Academic Press, 1980, 335-339.
19. Siegman, A. E., An Introduction to Lasers and Masers, New York: McGraw-Hill, 1971, 100, 103.
20. Perram, Glen P. "Characterization of an HF-Pumped CO₂ Laser," AFIT/GEP/PH/81D-7, October 1981, 5-15.
21. Pummer, H., Proch, D., Schmailzl, U., and Kompa, K. L., "The Generation of Partial and Total Vibrational Inversion in Colliding Molecular Systems Initiated by IR-Laser Absorption," Optics Communications, 19, 273-275, November, 1976.
22. Gross, R. W. F. and Bott, J. F., Handbook of Chemical Lasers, New York: John Wiley and Sons, 1976, 488-489.
23. Operating and Maintenance Manual, Line Tunable Fundamental Mode HF/DF Laser, Ottawa: Lumonics Research Limited, 1973.
24. Lindquist, G. H., Peterson, L. M., and Arnold, C. B., "Rotational Relaxation Measurements and Resonant Phenomena in Laser-Excited Hydrogen Fluoride," 101300-18-F, June 1974, Environmental Research Institute of Michigan Infrared and Optics Division, Ann Arbor, Mi.
25. Pummer, H., Proch, D., Schmailzl, U., and Kompa, K. L., "IR-Laser-Induced Collisional Pumping of Small Molecules: I. General Discussion and Experimental Results for Hydrogen Fluoride," Journal of Physics, Department: Applied Physics, 2, 102-104, 1978.
26. Kerber, Ronald L. and Whittier, James S., Simple Model of a Chain-Reaction Pulsed HF Laser. SAMSO-TR-77-154. Los Angeles, California: Space and Missile Systems Organization, Air Force Systems Command, July 1977.

27. Osgood, R. M. Jr., Javin, A., and Sackett, P. B., "Measurements of Vibration-Vibration Energy Transfer Time in HF Gas," Applied Physics Letters, 20, 470, June 1972.
28. Spiegel, Murray R. A., Advanced Mathematics For Engineers and Scientists, New York: McGraw-Hill Book Company, Schaum's Outline Series in Mathematics, 1971, 40.
29. Schmailzl, U., Pummer, H., Proch, D., and Kompa, K. L., "IR-Laser Induced Collisional Pumping of Small Molecules: II. Modelling," Journal of Physics, Department: Applied Physics, 2, 122-123, 1978.
30. Jursich, G. M. and Crim, F. F., "Vibrational Relaxation of HF ($v=3,4,5$)," Journal of Chemical Physics, 74, 4456-4457, April 1981.
31. Osgood, R. M. Jr., Sackett, P. B., and Javin, A., "Measurement of V-V Transfer Rates From HF $V=3$ Using Simultaneous Optical Pumping on the HF $V=2 \rightarrow 1$ and $V=1 \rightarrow 0$ Bands," Applied Physics Letters, 22, 254, March 1973.
32. Chen, Francis F., Introduction to Plasma Physics, New York: Plenum Press, 1977, 1-3.
33. Samaras, Demetrios G., Theory of Ion Flow Dynamics, Englewood Cliffs, New Jersey: Prentice-Hall, Inc., 1962, 163.
34. Ashmore, P. G. and Donovan, R. J., Gas Kinetics and Energy Transfer, Vol 3. London: Burlington House, The Chemical Society, 1978, 120.
35. Operating and Service Manual, Model 162 Boxcar Integrator, Princeton, New Jersey: EG&G Princeton Applied Research, 1980.
36. Discussion with Joe Brondelik, Air Force Wright Avionics Laboratory, AFWAL/AADO-1, Wright-Patterson Air Force Base, Ohio, 45433.
37. Klein, Miles V., Optics, New York: John Wiley & Sons, 1970, 570-573.
38. Henghold, Robert L., Professor, Air Force Institute of Technology, Class notes from Ph 6.42, Spring Quarter, 1982.
39. Operating and Service Manual, Model 162 Gated Integrator, Princeton, New Jersey: EG&G Princeton Applied Research, 1980, IV-1-19.
40. Dressley, Robert J., Ed. CRC Handbook of Lasers with Selected Data on Optical Techniques. Cleveland: Chemical Rubber Company, 1971.
41. Wolf, W. L. and Zissis, George J., ed. The Infra Red Handbook. Infra Red Information and Analysis Center, Environmental Research Institute of Michigan, 1978.

42. Handcock, J. and Green, W. H., "Vibrational Deactivation of HF ($v=1$) in Pure HF and in HF-Additive Mixtures," Journal of Chemical Physics, 57, 4515-4518, 1972.
43. Blauer, J. A., Solomon, W. C., Sentman, L. H., and Owens, T. W., Catalytic Efficiencies of H_2O , D_2O , NO , and HCl in the Vibrational Relaxation of HF and DF," Journal of Chemical Physics, 57, 3278-3279, 1972.

Appendix A

HF Lumonics Model TE-112 laser operating instructions

This appendix lists the turnon procedure used in this study for the HF pump laser.

- 1) check oil level in exhaust pump
- 2) check and close line valves
- 3) open tank valves on He, O₂, SF₆, N₂ and H₂
- 4) turn on AC at laser console
- 5) start exhaust pump
- 6) close pump throttling valve on console
- 7) open console gas lines
- 8) press gas on (console), allow to purge
- 9) close console gas lines
- 10) adjust nitrogen controls on back of laser cabinet to 0.8
- 11) open sulphur hexafluoride line valve
- 12) open console valve for sulphur hexafluoride to 25
- 13) open helium and oxygen line valves
- 14) open helium/oxygen console valve to 7.5
- 15) open hydrogen line valve
- 16) open hydrogen console valve to 5.5
- 17) open pump throttle to between 60 and 70 torr
- 18) turn on high voltage (push button on cable)
- 19) set variac to between 30 KV and 35 KV
- 20) set repetition rate to desired rate
- 21) check beam position
 - a) adjust position by rear grating vernier
 - b) set beam to point by front element adjustments

The shutdown procedure is

- 1) reduce variac to zero
- 2) HV off
- 3) close tank gas lines (hydrogen first), allow to purge
- 4) close console gas lines
- 5) turn off console gas
- 6) close line valves
- 7) turn off nitrogen control on laser
- 8) turn off pump
- 9) turn off console power

Appendix B

Computer program listings

This appendix lists two computer programs used to obtain rate constants for V-V exchanges and intensities in the reference and ORTL cells. The programs were run on a Sinclair ZX-81 microcomputer with 16K ram.

```
1 REM "ORTL"
5 REM OPTICAL RESONANCE
6 REM TRANSFER LASER
7 REM VIBRATIONAL RATE CONSTANT PROGRAM
8 REM CALCULATE ENERGY IN INVERSE
9 REM CENTIMETERS
10 DIM D(7)
20 DIM E(7)
110 LET WE = 4138.52
120 LET XEWE = 90.06
130 LET YEWE = 0.980
140 LET ZEWE = 0.025
150 LET BE = 20.939
160 LET AE = 0.770
170 LET CE = 0.005
180 LET D(1) = 0.0022
190 LET D(2) = 0.001
200 LET D(3) = 0.003
210 LET D(4) = 0.002
220 LET D(5) = 0.001
230 LET ZE = ZEWE/WE
240 LET XE = XEWE/WE
250 LET YE = YEWE/WE
260 FOR V = 0 TO 6
270 LET V1 = V+1/2
280 REM ZX81 CANNOT HANDLE 0
290 REM SUBSCRIPT
300 LET E(V+1) = V1*WE*(1-XE*V1+YE*V1*V1-ZE*V1*V1*V1)
310 NEXT V
320 LET N = 5.3416051E13
330 LET C = 4.307E-3
340 LET X = 7.58
350 LET V = 2
360 REM MODEL FOR V-V
370 REM ENERGY TRANSFER RATE
```

```

390 LET AR = N*((V-1)**X)
400 LET AK = (E(V+1)+E(3)-E(V)-E(4))
410 LET AK1 = (E(V+1)+E(4)-E(V)-E(5))
420 LET AK2 = (E(V+1)+E(5)-E(V)-E(6))
430 LET AK3 = (E(VH)+E(6)-E(V)-E(7))
440 LET K = AR*EXP(-C*AK)
450 LET L = AR*EXP(-C*AK1)
460 LET M = AR*EXP(-C*AK2)
470 LET O = AR*EXP(-C*AK3)
480 PRINT "KAC";V-1;"=";K;"CC/MOL-SEC"
490 PRINT
500 PRINT "KB
510 PRINT
520 PRINT "KC
530 PRINT
540 PRINT "KD
550 LET PR = 1.5E12*SQR(300)
560 PRINT
565 PRINT "AEROSPACE CORP. KINETIC RATE CONSTANTS"
570 PRINT "KA = ";PR
580 PRINT "KB = ";PR/2
590 PRINT "KC = ";PR/4
600 PRINT "KD = ";PR/8
610 PRINT
620 LET T2 = ((PR/2)-L)*100/(PR/2)
630 LET T3 = ((PR/4)-M)*100/(PR/9)
640 LET T4 = ((PR/8)-O)*100/(PR/8)
650 PRINT "ERRORS"
660 PRINT T2
670 PRINT T3
680 PRINT T4
690 STOP

```

```

1 REM "FRESNEL"
80 PRINT "REFRACTIVE INDEX 1?"
90 INPUT N1
100 PRINT "REFRACTIVE INDEX 2?"
110 INPUT N2
120 PRINT "DO YOU WANT BREWSTER'S ANGLE?"
130 INPUT T$
140 IF T$ = "N" THEN GOTO 190
150 LET THI = ATN N2
160 LET SNELL = N1*(SIN THI)/N2
170 LET THT = ASN SNELL
175 PRINT THI
180 GOTO 220
190 PRINT "INCIDENT ANGLE?"
200 INPUT THI
205 LET THI = (THI/180)*Pi
210 GOTO 160
220 LET STH = THI+THT
225 LET RPER = SIN(THI-THT)
230 LET RPERP = (RPER*RPER)/((SINSTH)**2)
240 IF STH > 1.569 THEN LET STH = 1.569
245 LET RPAR = TAN(THI-THT)
250 LET RPARA = (RPAR*RPAR)/((TANSTH)**2)
260 LET TPARA = 1-RPARA
270 LET TPERP = 1-RPERP
280 PRINT "REFLECTION // TO POI="
290 PRINT RPARA
300 PRINT "REFLECTION NORMAL TO POI="
310 PRINT RPERP
320 PRINT "TRANSMITTED // TO POI="
330 PRINT TPARA
340 PRINT "TRANSMITTED NORMAL TO POI="
350 PRINT TPERP
360 STOP

```

Appendix C

Electronics equipment listing/settings for Boxcar Averager.

This appendix lists the electronics equipment used in the ORTL experiment. The equipment used is as follows:

Perkin Elmer Model E-1 monochrometer
Hewlet Packard Model 184 Storage Oscilloscope
EG&G PAR Model 162 Boxcar Averager
EG&G PAR Model 165 Gated Integrator (two used)
Hewlet Packard model 7004 X-Y plotter
Santa Barbara InSb detector/preamp (ser# 3478)
S.A.T. HgCdTe detector
Lambda 15V DC power supply

The settings used on the EG&G models 165 and 162 Boxcar averager are given in Table VI.

Table VI

Model 165	Channel A	Channel B
Time Constant	10 μ sec	10 μ sec
Base Line Delay	0	0
Aperture Duration	out	out
Averaging	exp	exp
DC coupling	in	in
Input impedance	10K	10K
Sensitivity	500mV	100mV
Model 162		
Aperture delay range	1 micro second (initial % A and B = 0.5%)	
Aperture duration	50 n second	
Scan Time	1000 seconds	
Functions	A, B, A/ B , Log (A /B)	
Time Constant	100 seconds (MAX)	
Trigger mode	external	
Scan select	A, single scan	

Appendix D

Fresnel's Equations

These equations are used to determine the intensities of reflected and transmitted portions of the pump beam. The numerical solution was obtained using a Sinclair ZC-81 microcomputer. A listing of the code is contained in Appendix B.

Consider a pump laser beam with a power per unit area given by

$$\vec{S} = c^2 \epsilon_0 \vec{E} \times \vec{B}$$

Then the radias flux density is

$$I = \langle \vec{S} \rangle = \frac{c \epsilon_0}{2} E_0^2$$

The reflectance, R is now

$$R = \frac{I_r \cos \theta_r}{I_i \cos \theta_i} = \frac{I_r}{I_i}$$

where θ_i is the angle of incidence on a plane and θ_r is the angle of reflectance. Similarly, the transmittance, T is given by

$$T = \frac{I_t \cos \theta_t}{I_i \cos \theta_i}$$

where θ_t is the angle of transmission. Then the component of R perpendicular to the plane of incidence is given by

$$R_{\perp POI} = \left[\frac{\sin(\theta_i - \theta_t)}{\sin(\theta_i + \theta_t)} \right]^2$$

and the component of R parallel to the plane of incidence is given by

$$R_{//POI} = \left[\frac{\tan(\theta_i - \theta_t)}{\tan(\theta_i + \theta_t)} \right]^2$$

The components of transmittance are found by

$$T_{\perp POI} = 1 - R_{\perp POI}$$

and

$$T_{//POI} = 1 - R_{//POI}$$

[14:74, 79-80]

Appendix E

The Temperature of the Gas in the ORTL Cell

The temperature of the gas was calculated assuming R-T (HF-He) to be fast compared to V-V (HF-HF) [21:273-274]. Using the equation of state

$$PV = nkT$$

$$p = 66644.8 \text{ dynes/cm}^2 \text{ or } 50 \text{ torr of He}$$

$$v = 3.5628 \text{ cm}^3$$

$$T = 295K$$

$$\text{then } n = 5.8325 \times 10^{18} \text{ molecules}$$

The power per pulse was measured over 96 pulses to be 130×10^{-3} J/sec in one minute or 0.081 Joules. In Chapter III, the pump was calculated to be 92.7% of the pulse or 0.0753 Joules. Now

$$E = nkT \quad [9:26]$$

$$\text{or } 0.0753 \text{ J} = 5.8325 \times 10^{18} kT$$

$$T = 931.8K$$

Appendix F

Refractive Index Calculations

The values of the refractive index for silicon and zinc selenide were obtained by the following formulas:

$$\text{S: } n = A + BL + CL^2 + D\lambda^2 + E\lambda^4$$

$$A = 3.14696$$

$$B = 0.138497$$

$$C = 0.013924$$

$$D = -0.0000209$$

$$E = 0.000000148$$

$$L = (\lambda^2 - 0.028)^{-1} \quad [41:7-76]$$

ZnSe

$$n^2 - 1 = 2.855 + 2.045\lambda^2 / (\lambda^2 - 0.109)$$

[40:520].

AD-A124 708

CHARACTERIZATION OF A PULSED HF OPTICAL RESONANCE
TRANSFER LASER(U) AIR FORCE INST OF TECH

2/2

WRIGHT-PATTERSON AFB OH SCHOOL OF ENGINEERING D A RUDD

UNCLASSIFIED OCT 82 AFIT/GEP/PH/82D-20

F/G 20/5

NL

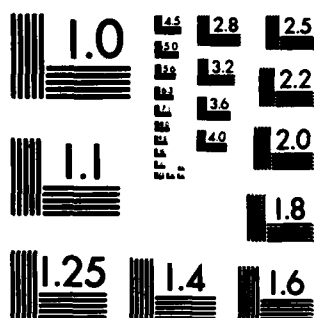


END

DATE

FILED

DTIC



MICROCOPY RESOLUTION TEST CHART
NATIONAL BUREAU OF STANDARDS-1963-A

Appendix G

Photon number calculations

An ORTL cell run in CW mode (typical) has the following characteristics:

- (a) 2.3cm x 0.38cm cross section and 1cm deep with a 5×10^3 cm/
second flow rate. The effective volume is then
 $2.3 \times 0.38 \times 1.0 \times 5 \times 10^3$ cm³/sec.
- (b) The beam is passed three times through the medium.
- (c) The beam has 310 watts of power (typical) for 3% HF in helium
with a total pressure of 40 to 110 torr [17:1]

now consider the following:

$$\frac{310 \text{ watts}}{2.3 \times 0.38 \times 5 \times 10^3 \text{ cm}^3/\text{sec}} = 71 \times 10^{-3} \text{ J/cm}^3$$

for 1/2 torr of HF there are approximately 8.2×10^{15} molecules/cm³ in
1cm³ volume at about 600K.

$$\text{Then } \frac{71 \times 10^{-3} \text{ J/cm}^3}{8.2 \times 10^{15} \text{ molecule/cm}^3} = 8.7 \times 10^{-18} \text{ J/molecule}$$

$$\text{At } 2.8\mu, h\nu = 6.626 \times 10^{-34} \times 1.079 \times 10^{14} = 7.15 \times 10^{-20} \text{ J/photon}$$

Then in CW it is required that

$$\frac{8.7 \times 10^{-18}}{7.15 \times 10^{-20}} = 122 \text{ photons/molecule}$$

for a single pass and thus 366 photons/molecule for three passes.

The following modifications are needed for the pulsed ORTL: The
fluorescence decay rate for HF is approximately 8×10^4 /sec-torr. At
1/2 torr this is 4×10^4 /sec-torr [15:5541]. Then for input pulses

considerably shorter than $(4 \times 10^4)^{-1}$ consider the power factor reduction based on the probability for relaxation of HF. This is not an exact calculation and does not take into consideration saturation or bleaching. The probability for HF-HF vibrational relaxation is $\approx 8 \times 10^{-3}$ at 295K [13:1028]. Then for a short input pulse an ORTL condition is assumed to exist if there are about

$$(366) \times (8 \times 10^{-3}) \approx 3 \text{ photons/molecule}$$

This is only an order of magnitude calculation.

VITA

Douglas Allen Rudd was born on 27 August 1945 in Orlando, Florida. He graduated from Clermont High School in Clermont, Florida in 1963 and attended Lake-Sumter Junior College before entering the Air Force in 1966. After leaving the Air Force in 1970 he worked in radiology and then entered the University of South Florida where he received the degrees of Bachelor of Arts in Geology and Bachelor of Science in Physics in June 1978. He then worked as a hydrogeologist before entering the Officer Training School in March 1979. He was commissioned in June 1979 and was assigned to the Air Force Weapons Laboratory, Kirtland Air Force Base, New Mexico. There he worked in the Chemical Laser Branch in computational analysis and program management. He was assigned to the School of Engineering, Air Force Institute of Technology in June 1981.

Permanent address: 1003A Courtney Drive
Dayton, Ohio 45431

UNCLASSIFIED

SECURITY CLASSIFICATION OF THIS PAGE (When Data Entered)

REPORT DOCUMENTATION PAGE		READ INSTRUCTIONS BEFORE COMPLETING FORM
1. REPORT NUMBER AFIT/GEP/PH/82D-20	2. GOVT ACCESSION NO. AD-A124708	3. RECIPIENT'S CATALOG NUMBER
4. TITLE (and Subtitle) CHARACTERIZATION OF A PULSED HF OPTICAL RESONANCE TRANSFER LASER		5. TYPE OF REPORT & PERIOD COVERED MS Thesis
7. AUTHOR(s) Douglas A. Rudd 1Lt USAF		6. PERFORMING ORG. REPORT NUMBER
9. PERFORMING ORGANIZATION NAME AND ADDRESS Air Force Institute of Technology (AFIT/ENA) Wright-Patterson AFB, Ohio 45433		8. CONTRACT OR GRANT NUMBER(s)
11. CONTROLLING OFFICE NAME AND ADDRESS		10. PROGRAM ELEMENT, PROJECT, TASK AREA & WORK UNIT NUMBERS
14. MONITORING AGENCY NAME & ADDRESS (if different from Controlling Office)		12. REPORT DATE December, 1982
		13. NUMBER OF PAGES 89
		15. SECURITY CLASS. (of this report) Unclassified
		15a. DECLASSIFICATION/DOWNGRADING SCHEDULE
16. DISTRIBUTION STATEMENT (of this Report) Approved for public release; distribution unlimited		
17. DISTRIBUTION STATEMENT (of the abstract entered in Block 20, if different from Report) Approved for public release: IAW AFR 130-17. LYNN E. WOLAVER Dean for Research and Professional Development Air Force Institute of Technology (AIC) Wright-Patterson AFB OH 45433 4 JAN 1983		
18. SUPPLEMENTARY NOTES Prepared in cooperation with the Avionics Laboratory, AFWAL, WPAFB, OH 45433 (Dr. W. Schuebel and J. Brandelik/AADO/AFWAL).		
19. KEY WORDS (Continue on reverse side if necessary and identify by block number) HF Pumped Optical Resonance Transfer Laser, Pulsed HF Optical Resonance Transfer Laser.		
20. ABSTRACT (Continue on reverse side if necessary and identify by block number) The HF ($v=2$) vibrational level was pumped optically on the $P_2(8)$ transition and $P_2(7)$ transition. The 0.5 percent HF in helium gas at 50 torr was pumped by an HF laser with 0.081 joules per pulse and 96 pulses per second. The technique involves observation of absorption by HF ($v=2$). Decreased absorption was observed on the $P_2(8)$ transition implying the possibility of gain by V-V exchange. The data shows conformance with the results of a previous investigation on the $P_2(8)$ line. Interrogation of the $P_2(7)$ transition failed to yield conclusive results due to a poor signal to noise ratio.		

DD FORM 1 JAN 73 1473

EDITION OF 1 NOV 65 IS OBSOLETE

UNCLASSIFIED

SECURITY CLASSIFICATION OF THIS PAGE (When Data Entered)

UNCLASSIFIED

SECURITY CLASSIFICATION OF THIS PAGE(When Data Entered)

A theoretical model of the kinetics of the HF V-V and V-T exchanges was established. Pulse shapes predicted by this theory and those observed experimentally for the $P_2(8)$ line agree well.

Excessive noise levels precluded investigation of other transitions.

UNCLASSIFIED

SECURITY CLASSIFICATION OF THIS PAGE(When Data Entered)